https://doi.org/10.61092/iaea.j0qb-ddr7

INDC(NDS)-0772
Distr. G,NM,PH

IAEA
International Atomic Energy Agency

INDC International Nuclear Data Committee

Revision and Update of Experimental Gamma-ray Strength Functions Derived from the Discrete Neutron Resonance Capture

Jiri Kopecky
JUKO Research
Alkmaar, The Netherlands

December 2018

IAEA Nuclear Data Section
Vienna International Centre, P.O. Box 100, 1400 Vienna, Austria

Selected INDC documents may be downloaded in electronic form
from *http://nds.iaea.org/publications*
or sent as an e-mail attachment.
Requests for hardcopy or e-mail transmittal should be directed to
NDS.Contact-Point@iaea.org
or to:
Nuclear Data Section
International Atomic Energy Agency
Vienna International Centre
PO Box 100
1400 Vienna
Austria

Printed by the IAEA in Austria

December 2018

INDC(NDS)-0772
Distr. G,NM,PH

Revision and Update of Experimental Gamma-ray Strength Functions Derived from the Discrete Neutron Resonance Capture

Jiri Kopecky
JUKO Research
Alkmaar, The Netherlands

December 2018

Contents

1. Introduction 7
2. Survey of early DRC measurements 7
3. Processing DRC data in the PSF format 13
3.1. Discussion of results 19
4. Processing the quasi-mono energetic strength functions 22
4.1. Discussion of results 29
4.2. Comparison with previous DRC analysis 34
4.3 Comparison with PSF model (QRPA approach) 37
5. Conclusions and recommendations 40
5.1. The absolute calibration of the E1 strength 41
5.2. Recommendation 42

APPENDIX – DRC Data Sources 45

1. Introduction

Properties of neutron resonances have been one of the most exciting and widely spread fields of low energy neutron nuclear physics. From 1960 onwards, the resonance behavior of neutron interaction with matter was studied in many laboratories using the white TOF spectra at accelerators or reactors. General interest in resonance properties lasted about 30 years and was later replaced by studies of materials important for applications only. During those 30 years, the traditional transmission experiments were often extended by neutron capture measurements in discrete resonances – *Discrete Resonance Capture (DRC)* - primarily used as a spectroscopy tool to study initial and final states or the product nuclide. In some cases, the gamma decay properties, the gamma strength behavior of different multipole radiation was addressed, following the realization that this may give an interesting insight into the rules governing the gamma ray de-excitation of the target nucleus at energies below the reaction threshold and how it connects to the photonuclear tail of the Giant Dipole Resonance (GDR). Furthermore, the DRC data are the only direct tool for the absolute normalization of Average Resonance Capture (ARC) measurements.

2. Survey of early DRC measurements

Laboratories involved in *DRC* type of measurements were ORNL, LNL and BNL in the US, Chalk River in Canada and at UKAEA Harwell, JINR Dubna and IRM Geel in Europe. The most recent measurements have been carried out in Dubna and Geel during the second half of the nineteen eighties. The pioneering group with the largest data production was the Neutron Physics Group at BNL headed by R.E. Chrien. It did not come as a surprise that this group, in 1981, published the first comprehensive collection of DRC data to compare the experimental gamma-ray decay properties with the predictions of the Single Particle (SP) or Giant Resonance Models (GRM)[1]. The main output of this work was a data set of binned model dependent k(E1, M1) or S(E1) strength function values, averaged not only over measured resonances, but also over a number of gamma transitions in order to increase the averaging power, often limited due to a small number of resonances. The first survey was published by C. McCullagh et al. in 1981 [2]. This data base was later taken over by ECN in the frame of the BNL/ECN collaboration.

This collaboration resulted in several updates, starting in 1990 and extending until 1994, the extended data set has been reported in [3]. At this point a model independent definition of the photon strength function (PSF) was also employed, given by the equation

$$f(L)_i = \Gamma_{\gamma i} / E_{\gamma i}^3 D_l , \qquad (1)$$

where $\Gamma_{\gamma i}$, $E_{\gamma i}$ and D_l are standing for radiative width, primary transition energy and resonance spacing, respectively. This compilation was included in all RIPL documents [4-6] and remained unchanged through all releases up to 2009. It was based on the work of McCullagh et al. [2] from 1981, extended by Kopecky [3] with measurements between 1981 and 1994. In the latest revision,

the earlier D values were updated using the BNL Atlas of Neutron Resonances 2006 [7] and published in [8].

The final listing of entries from [8] has been extracted and used as a starter file for validation of parameters for new processing. This survey resulted in the total number of 57 nuclides ranging from ^{20}F up to ^{240}Pu and the full listing with references is shown in Table 1. The measured data include mainly s- resonances with the exception of the low mass region (A < 100) where many p-resonances from the 3p neutron strength function giant resonance are present. The time spread of publications ranges from 1967 up to 2003, however, the majority of experiments were carried out in the period from 1970 to 1985. Only s- and p- wave resonances were considered, a small number of d-wave resonances at very low A targets was used for ^{25}Mg and ^{29}Si nuclides only.

The format of the measured transition rate is also shown in Table 1, because this quantity forms the starting experimental information for the processing and conversion of these data into PSF format. The absolute calibration of the transition rate is taken from the original references and is considered as frozen. No attempt has been made to reopen this procedure.

TABLE 1 List of DRC measurements

#res - number of resonances, E1 and M1 transitions
l_n - neutron orbital momentum of resonances
Ref. DRC - given in a special section in Appendix
Tran. rate - absolute intensity/neutron capture ($I_{\gamma i}$) or partial radiative width ($\Gamma_{\gamma i}$) in eV
$\Gamma_{\gamma i*}$ - stands for transition strength expressed in the GRM model formalism see Ref. [1]

Product nuclide	**#res**	**l_n**	**Ref. DRC**	**Transition rate**
F-20	2	p	[1]	$I_{\gamma\iota}$
Mg-25	1	p	[2]	$I_{\gamma\iota}$
Al-28	2	s	[3]	$I_{\gamma\iota}$
Si-29	2	P	[4]	$I_{\gamma\iota}$
Si-30	1	P	[4]	$I_{\gamma\iota}$
S-33	1	P	[1]	$I_{\gamma\iota}$
Cl-36	1	p	[3] [5]	$I_{\gamma\iota}$
Sc-46	2	s	[6]	$\Gamma_{\gamma\iota}$*
Cr-53	1	p	[7]	$I_{\gamma\iota}$
Cr-54	23	s+p	[8]	$\Gamma_{\gamma\iota}$*
Fe-57	1	p	[9]	$\Gamma_{\gamma\iota}$
Fe-59	2	p	[10]	$I_{\gamma\iota}$
Co-60	1	s	[11]	$\Gamma_{\gamma\iota}$

Product nuclide	**#res**	**l_n**	**Ref. DRC**	**Transition rate**
Cu-64	3	s	[12]	$I_{\gamma\iota}$
Ge-74	5	s	[13]	$I_{\gamma\iota}$
Nb-94	7	s+p	[14]	$\Gamma_{\gamma\iota}$
Mo-93	9	s+p	[15]	$\Gamma_{\gamma\iota}$
Mo-99	17	s+p	[16]	$I_{\gamma\iota}$
Ru-100	4	s	[17][18]	$\Gamma_{\gamma\iota}$
Ru-102	6	s	[17][18]	$\Gamma_{\gamma\iota}$
Rh-104	6	s	[19]	$I_{\gamma\iota}$
Pd-106	8	s	[3][20]	$\Gamma_{\gamma\iota}$
In-116	31	s	[21]	$I_{\gamma\iota}$
Sb-122	12	s	[22]	$I_{\gamma\iota}$
Sb-124	4	s	[22]	$I_{\gamma\iota}$
Te-126	6	s	[3]	$\Gamma_{\gamma\iota}$
I-128	8	s	[3]	$I_{\gamma\iota}$
Ba-136	6	s	[3]	$\Gamma_{\gamma\iota}$
Nd-144	10	s	[3]	$\Gamma_{\gamma\iota}$
Nd-146	10	s	[23]	na
Sm-148	12	s	[24]	$I_{\gamma\iota}$
Sm-150	3	s	[25][26]	$I_{\gamma\iota}$
Gd-153		s	[26]	$\Gamma_{\gamma\iota}$*
Gd-155	15	s	[27]	$\Gamma_{\gamma\iota}$*
Gd-157	na	s	[26]	$\Gamma_{\gamma\iota}$*
Gd-159	12	s	[26][28]	$I_{\gamma\iota}$
Er-168	45	s	[30]	$\Gamma_{\gamma\iota}$
Er-169	7	s	[31]	$\Gamma_{\gamma\iota}$
Tm-170	9	s	[32]	$I_{\gamma\iota}$
Lu-176	11	s	[33]	$I_{\gamma\iota}$
Lu-177	6	s	[26] [34]	$I_{\gamma\iota}$
Yb-174	22	s	[15] [34]	$\Gamma_{\gamma\iota}$*
Hf-178	37	s	[35]	$I_{\gamma\iota}$
Ta-182	19	s	[3][36]	$\Gamma_{\gamma\iota}$*
W-183	7	s	[3]	$I_{\gamma\iota}$
W-184	6	s	[3]	$I_{\gamma\iota}$
Pt-196	22	s	[37]	$\Gamma_{\gamma\iota}$*

Product nuclide	**#res**	**l_n**	**Ref. DRC**	**Transition rate**
Au-198	4	s	[38]	$I_{\gamma\iota}$
Hg-199	2	s	[39]	$I_{\gamma\iota}$
Hg-200	3	s	[39]	$I_{\gamma\iota}$
Hg-202	3	s	[39]	$I_{\gamma\iota}$
Th-233	5	s	[40]	$I_{\gamma\iota}$
U-235	4	s	[40]	$\Gamma_{\gamma\iota}$
U-236	19	s	[41]	$I_{\gamma\iota}$
U-237	7	s	[3][42]	$\Gamma_{\gamma\iota}$
U-239	23	s	[43]	$\Gamma_{\gamma\iota}$
Pu-240	7	**s**	[44]	$\Gamma_{\gamma\iota}$

The following parameters, relevant for data processing, have been reviewed and, where necessary, updated:

1. The resonance angular momentum l_n, initial spin $J_{\pi i}$, the average capture width $<\Gamma_\gamma>_{s,p}$ and the partial width $\Gamma_{\gamma i}$ values.
2. The absolute values of D_0 or D_1 used in the original compilations [2,3], have been updated several times and have therefore been the primary focus for the present recalculation. Two latest D compilations have been reviewed in [8] and the conclusions were carefully re-examined in this work with respect to the latest release of *Atlas of Neutron Resonances* from 2018 [9]. Lacking any comprehensive experimental knowledge of the spin dependence of level spacing D(J), in cases where needed, the estimate based on the (2J+1) dependence of the level density was applied.
3. The parameters of the final states of the product nucleus, such as their spin J_f and the parity π, have been verified against the ENDSF data base [10]. These parameters play an important role in the classification of measured primary transitions to E1, M1 or E2 modes.

Results of this analysis are summarized in Table 2. The neutron spacing from the two latest independent compilations is shown, in order to indicate possible additional uncertainty due to conflicting spacing. Those cases are printed in bold. For unknown values the symbol “na” is used.

TABLE 2 Neutron resonance parameters of present DRC measurements

Product nuclide	**#res**	**l_n**	**J_t**	**J_i^-(#)**	**J_i^+(#)**	**D [eV] RIPL-3**	**D [eV] BNL-2018**
F-20	2	1	½+	1- (1)	2- (1)	60000	60 000
Mg-25	2	1 2	0+	3/2-(1)	 3/2+ (1)	16000	158 000 110000
Al-28	2	0 1	5/2+	2+ (1) 2- (1)		55000 27500	53700 28400
Si-29	1	1	0+	½- (1)		**75000**	**109000**
Si-30	1	1	½+	2- (1)		**85400**	**52400**
S-33	1	1	0+	½- (1)		46300	46300
Cl-36	1	1	3/2+	2- (1)		**6600**	**22300**
Sc-46	2	0	7/2-	3+ (1)	4+ (1)	1030	1030
Cr-53	1	1	0+	3/2- (1)		**1030**	**10500**
Cr-54	8 15	0 1	3/2-	1- (3) 1+(3)2+(2)	2- (5) 3+ (10)	6700 3060	5960 3060
Fe-57	1	1	0+	½- (1)		7700	8210
Fe-59	2	1	0+	½- (na)	3/2- (na)	5030	5030
Co-60	1	0	7/2-	4- (1)		1450	1390
Cu-64	3	0	3/2-	1- (1)	2- (2)	700	722
Ge-74	6	0	9/2+	4+ (5)	5+ (1)	62	60.1
Nb-94	3 4	0 1	9/2+	4+ (3) 4- (2)	 5- (2)	94 50	84.8 42.4
Mo-93	7 16	0 1	0+	½+ (7) 1/2- (4)	 3/2-(12)	2700 900	2800 780
Mo-99	5 11	0 1	0+	½+ (5) 1/2- (3)	 3/2- (8)	1000 290	970 286
Ru-100	4	0	5/2+	2+ (1)	3+ (3)	25	21.7
Ru-102	6	0	5/2+	2+ (3)	3+ (3)	18	18.5
Rh-104	7	0	½-	0- (1)	1- (6)	32	24.2
Pd-106	9	0	5/2+	2+ (3)	3+ (6)	10.3	10.9
In-116	22	0	9/2+	4+ (11)	5+ (11)	9.5	9
Sb-122	12	0	5/2+	2+ (5)	3+ (7)	13	10
Sb-124	4	0	7/2+	3+ (2)	4+ (2)	24	24
Te-126	12	0	½+	0+ (4)	1+ (8)	43	42.7
I-128	8	0	5/2+	2+ (4)	3+ (4)	15	9.7
Ba-136	6	0	3/2+	1+ (4)	2+ (2)	40	40

Product nuclide	#res	l_n	J_t	J_i^-(#)	J_i^+(#)	D [eV] RIPL-3	D [eV] BNL-2018
Nd-144	9	0	7/2-	3- (5)	4- (4)	38	37.6
Nd-146	10	0	7/2-	3- na	4- na	17	17.8
Sm-148	23	0	7/2-	3- (12)	4- (11)	5.7	5.7
Sm-150	3	0	7/2-		4- (3)	2.4	2.2
Gd-153	na	0	0+	½+ na		14	13.5
Gd-155	15	0	0+	½+ (15)		14.5	13.8
Gd-157	na	0	0+	½+ na		30	30.5
Gd-159	12	0	0+	½+ (12)		82	87
Er-168	45	0	7/2+	3+ na	4+ na	4.2	4
Er-169	7	0	0+	½+ (7)		100	94
Tm-170	10	0	½+	0+ (2)	1+ (8)	8.5	7.28
Lu-176	12	0	7/2+	3+ (7)	4+ (5)	3.45	3.45
Lu-177	6	0	7-	15/2- (6)		1.61	1.61
Yb-174	23	0	5/2-	2- (9)	3- (14)	7.5	8.06
Hf-178	20	0	7/2-	3- (9)	4- (11)	2.4	2.4
Ta-182	19	0	7/2+	3+ (9)	4+ (10)	4.2	4.17
W-183	7	0	0+	½ +(7)		60	63.4
W-184	7	0	½+	0+ (2)	1+ (5)	12	12
Pt-196	22	0	½-	0- na	1- na	18	17
Au-198	4	0	3/2+	1+ (1)	2+ (3)	15.5	15.7
Hg-199	2	0	0+	½+ (2)		105	250
Hg-200	3	0	½-	0- (1)	1- (2)	80	100
Hg-202	3	0	3/2-	1- (2)	2- (1)	90	90
Th-233	5	0	0+	½+ (5)		16.5	15.82
U-235	3	0	0+	½+ (3)		11.2	10.92
U-236	20	0	7/2-	3- (8)	4- (12)	11.2	0.49
U-237	7	0	0+	½+ (7)		14	14.7
U-239	23	0	0+	½+ (23)		20.3	16.4
Pu-240	7	0	½+	1+ (8)		2.2	2.07

J_t and $J_i^{\pm}$ are spins of target nuclide and of resonances with neutron l_n from the surveyed experiments. Two columns with J_i(#) symbol give the number of resonances with the spin J_i of used resonances. This is important information for the use of the proper spacing in the averaging process.

3. Processing DRC data in the PSF format

The next step in processing the DRC data is the conversion of the measured transition rates, using equation (1), in the PSF format. The procedure was as follows:

1. The list of measured transitions was checked to confirm the assignment of primary transitions against the listing of final states and their spin and parity values from the ENSDF data base.
2. Only transitions with $I_\gamma > dI_\gamma$ were considered, transitions to final states not included in the ENSDF data base were not used for any conclusive PSF treatment.
3. The measured transition rates are usually given in absolute intensities per $I_\gamma/100$ or 1000 captured neutrons or in partial radiative widths $\Gamma_{\gamma i}$ in eV.
4. For the conversion of I_γ intensities to $\Gamma_{\gamma i}$ values the product of I_γ and Γ_γ was used, using either the average s- or p-wave Γ_γ width of all resonances or the partial width of discrete resonances in the DRC experiment. Values from [9] were adopted for both cases. It seems that both approaches, in view of all other uncertainties, differ negligibly and both can be safely used.
5. If the $\Gamma_{\gamma i}$ values are given in the data source, these values were adopted without any change. The reason for that is that the original I_γ could not be retrieved for recalculation and the applied Γ_γ are not usually quoted.
6. The average partial width $<\Gamma_\gamma>$ over measured resonances for a given transition is determined by an unweighted average over all resonances of the same spin and parity as in [2]. However, a partial width equal to zero may occur due to experimental sensitivity limits and Porter-Thomas fluctuations. This effect was accounted for in [2] by the application of missed intensity correction from the Porter-Thomas distribution using the intensity ratio of the smallest observed transition to the observed partial average width of this transition as an input parameter. This correction was in the present analysis neglected, for two reasons: In many data entries the extract of the above-mentioned ratio is not possible and, furthermore, even when there are enough transitions the effect is small [2]. However, for nuclides ($A > 50$) with a limited number of transitions, the average $<\Gamma_{\gamma i}>$ may slightly be increased due to this neglect.
7. Special care was devoted to l_n assignments of measured resonances, especially, for light nuclides.
8. The dependence of the spacing on the initial resonance spin has been taken into account for measurements with only one single resonance and/or for cases with more resonances but with only one spin value. See Section 3.

After implementation of the above steps, average partial radiative widths $<\Gamma_{\gamma i}>$ can be used in Eq. (1) to calculate the strength function. The average value of $<\Gamma_{\gamma i}>$ over measured resonances, reduced by the phase factor E_γ^3, and with $D_{0,1}$ value adopted from [9], then gives the average partial strength function $<f(L)_i>$ (see an example in Table 3) in units of 10^{-8} MeV^{-3} using Eq. (1). The

quoted uncertainties are standard errors based on standard error propagation (in quadrature) of statistical uncertainties from the gamma ray spectra analysis taken from the original sources if the transition strength was given in $\Gamma_{\gamma I}$. For some nuclides (with strength in I_γ) the statistical and normalization ($\Gamma_{\gamma i)}$ uncertainty was assumed to be 25%, as a conservative guess. The final data are given in Excel spreadsheets, similar to the ARC data [11] and stored in a data base called" ATLAS DRC f(L)" for 57 nuclides.

The data format is organized as follows: The basic information on the data source, transition strength units, measured resonances with used Γ_γ and resonance spacing is included in the heading. In case the original data source gives the transition strength in partial $\Gamma_{\gamma i}$ values, these results are directly adopted. Further the Porter-Thomas dispersion estimate 1+ dPT = 1 + $\sqrt{2}/\upsilon$, with υ = number of resonances, which can serve as a crude classification of the averaging power is shown. An example is given in Table 3.

TABLE 3 ^{198}Au entry in the "Atlas DRC f(L)" data base

Au-198 DRC data BNL

Iγ/1000 captures from O.A. Wasson et al., Phys.Rev. 173 (1968) 1170
4 s-resonances = (3 res. with J=2+ and one J=1+) Γγ0 = 0.128 Ev
D0=15.7 eV
Porter-Thomas dispersion estimate: 1+dPT =√2/υ=1.71
Statistical error assumed to be 25%

E(gamma)	E1	M1	E2	dE1	dM1	dE2	Ex	Jpi
6513	36.44			7.29			0	2-
6458	26.26			5.25			55	1-
6421							92	0-
6320	41.02			8.20			193	1-
6277	14.67			2.93			236	3-
6265	3.48			1.04			248	1-
6253	47.85			9.57			260	1-
6184	17.32			3.46			329	3-
6173	3.38			1.01			340	1-
6166	28.6			5.72			347	2-
6150	9.81			1.96			363	2-
6145	23.89			4.78			368	1-
6107	17			3.40			406	2-
6061	20.6			4.12			452	2-
6018	4.02			1.20			495	1-
5983	22.94			4.59			530	3-

5941	17.11		3.42		572	1-
5887	6.39		1.90		626	3-
5880	8.82		2.60		633	1-2-
5840	10.54		2.11		673	1-2-3-
5808	48.58		9.72		705	1-
5784	5.58		1.67		729	0-
5767	11.58		2.32		746	1-2-
5724	17.61		3.52		789	1-
5711	38.63		7.73		802	1-2-
5677	3.68		1.10		836	3-
5643	5.56		1.67		870	3-
5621	18.13		3.63		892	1-2-
5595	24.79		4.96		918	1-2-
5581	7.27		2.18		932	0-
5555	21.05		4.21		958	1-2-
5540	8.03		2.40		973	3-
5524	15.11		3.02		989	3-
5512	15.46		3.09		1001	1-2-
5494	17.7		3.54		1019	1-2-
5474	3.23		0.97		1039	1-2-
5463	14.38		2.88		1050	1-2-
5456	12.68		2.54		1057	2-
5419	5.76		1.73		1094	0-
5404	14.85		2.97		1109	1-2-
5396	3.89		1.17		1117	
5387	11.73		2.35		1126	1-2-
5365		6.34		1.90	1148	1+2+
5355	9.95		1.99		1158	3-
5346	9.47		1.89		1167	1-2-
5336	8.18		1.64		1177	1-2-
5308	16.49		3.30		1205	1-2-
5303	6.15		1.23		1210	3-
5280	7.75		2.32		1233	3-
5272	2.5		0.75		1241	3-
5256	14.04		2.81		1257	1-2-
5244	7.49		2.25		1269	
5231	1.42		0.43		1282	
5226	5.43		1.09		1287	2-
5223	0.57		0.17		1290	
5218	3.73		1.12		1295	1-2-
5206	11.7		2.34		1307	2-
5193	11.21		2.24		1320	1-2-

The majority of studied nuclides include a rather small number of resonances, often smaller than five and the averaging power is therefore rather limited, and the data dispersion is broad. An example of such a measurement is given in Fig.1 for ^{198}Au.

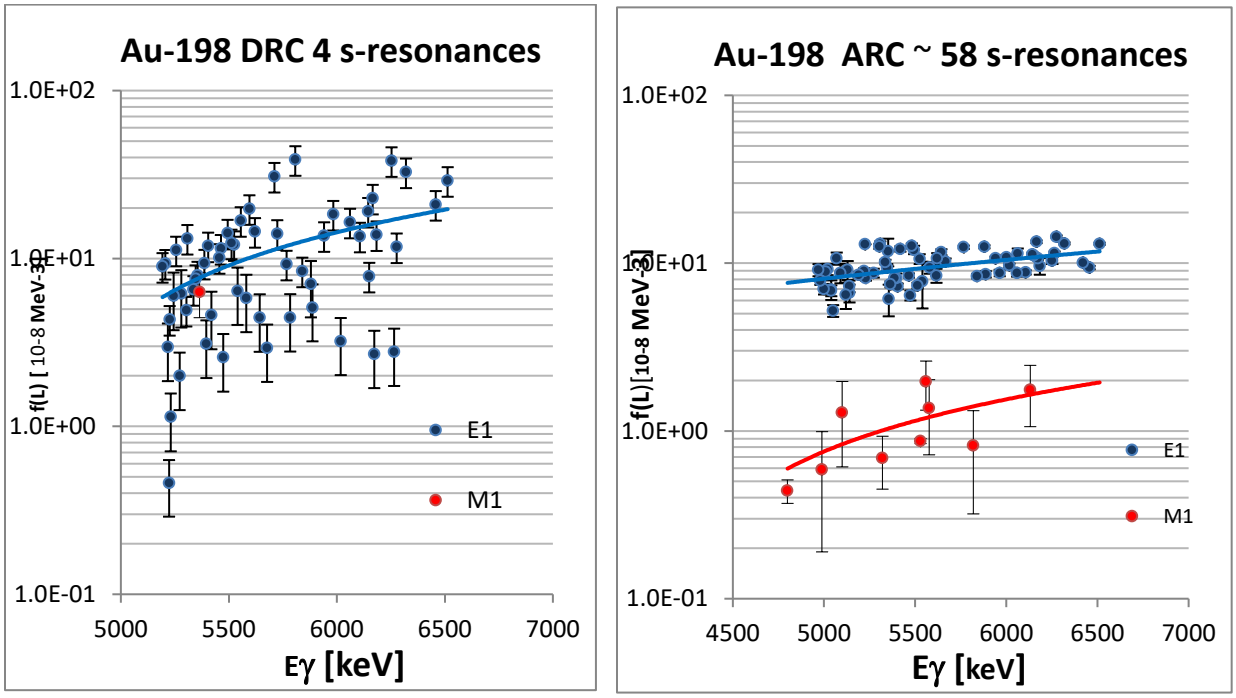

FIG. 1 *PSF partial data averaged over 4 s-wave resonances. Note the dispersion of E1 data over more than one order of magnitude, slightly more than the Porter-Thomas estimate. For a comparison with the filtered ARC beam experiment the plot of the same nuclide is shown from the Sc filter. Note the improvement in the dispersion and the detection of M1 transitions due to the higher flux of the filtered beam.*

Some features of averaging of DRC data are discussed, which may influence the dispersion of measured partial $f(L)_i$ values. A clarifying remark is needed to show the difference in averaging between two PSF experiments. In the filtered beam ARC experiments, the averaging over all resonances in a given neutron window is done by measuring the combined transition strength from all resonances. In the TOF DRC measurements, the transition strength of primary transitions is measured in discrete resonances and stored as such. The averaging over all measured resonances is then calculated as a mean value for N entries, where N is the number of measured resonances.

The first two reasons which cause the data dispersion are the statistical uncertainty of measured gamma ray intensities and the Porter-Thomas fluctuations of the transition strength, which is the major source of fluctuations. They both depend on to the physics of the experiment. The statistical

uncertainty depends on the quality of the experimental set-up (neutron flux, detection quality etc.) and is typically 5 – 20% for strong transitions and can be up to 50% for the very weak ones. The size of Porter-Thomas dispersion decreases by measuring more resonances and possibly also by averaging additionally over several gamma transitions. The Porter-Thomas fluctuations usually significantly dominate over the statistical fluctuations. Additional contributions to errors and uncertainties of derived $\langle f(L) \rangle_I$ are the uncertainties in the values of the total radiative width Γ_γ and the resonance level spacing D. They are typically of the order of 10 – 20%. They are not included in the quoted errors in Table 3 but are considered in the final data systematics.

Another source of the data dispersion is the multiple spins J_i of the initial states. If the initial resonance spin can have two values, e.g. $J_t \pm 1/2$ for s-wave resonance, the dipole transitions to outer spins ($J_t \pm 3/2$) can come from only one resonance spin (see Fig. 2 taken from [12]) and this has to be taken into account in the averaging procedure. For p-wave capture the situation is even more complicated.

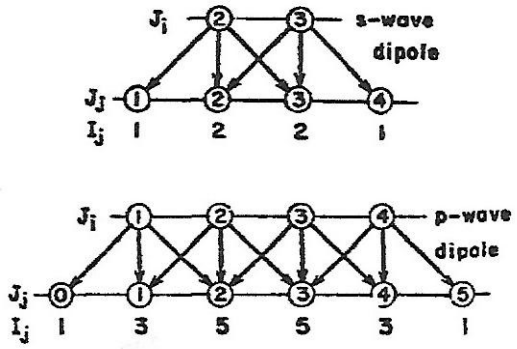

FIG. 2 *Schematic picture of multiple population from $J_i \pm 1/2$ and $J_i \pm 1/2 \pm 3/2$ final spins in s- or p-wave capture. The multiple population correction factors are shown as I_j estimates.*

This effect has been accounted for in the filtered beam experiments (ARC data) and corrected in the processing [11]. Due to the large number of resonances there usually is an equal number of initial spins present and the simplified correction factors, shown in Fig. 2 as I_j, can be applied as was confirmed by the Monte Carlo simulation [11]. However, an important condition has to be fulfilled, namely the value of the final spins J_j needs to be known unambiguously. This is usually only true for some of the highest primary transitions. Therefore, a few transitions remain uncorrected but due to the very large number of resonances that allow for efficient averaging of ARC experiments this does not severely influence the trend of the transition strength as a function of E_γ.

The situation is different with DRC experiments, where transitions from discrete resonances are measured and there is no multiple population of final states. The data can be processed (averaged) separately in groups with the same initial spin and later averaged over these groups. In several recent publications this approach is applied, and the final data are presented in separate J_i spin groups (Refs. [13-15]). However, this approach needs a reasonably large number of resonances, in order to make the second averaging (over spin groups) correct. If this condition is not fulfilled (e.g. for light mass nuclei or a measurement with small amount of transitions) the double averaging may be misleading due to the impact of the weight of strongly deviating entries. In such a case one should apply the I_j correction factors (as for ARC experiments) with caution.

A special approach was applied to nuclides with combined presence of s- and p-wave resonances. The corresponding data sets have been treated separately and are combined in one data set including E1 and M1 transitions where e.g. E1 transitions in the s-wave capture become pure M1 transitions in the p-wave capture. A typical example of such a situation is shown for ^{93}Mo in Figs. 3 and 4.

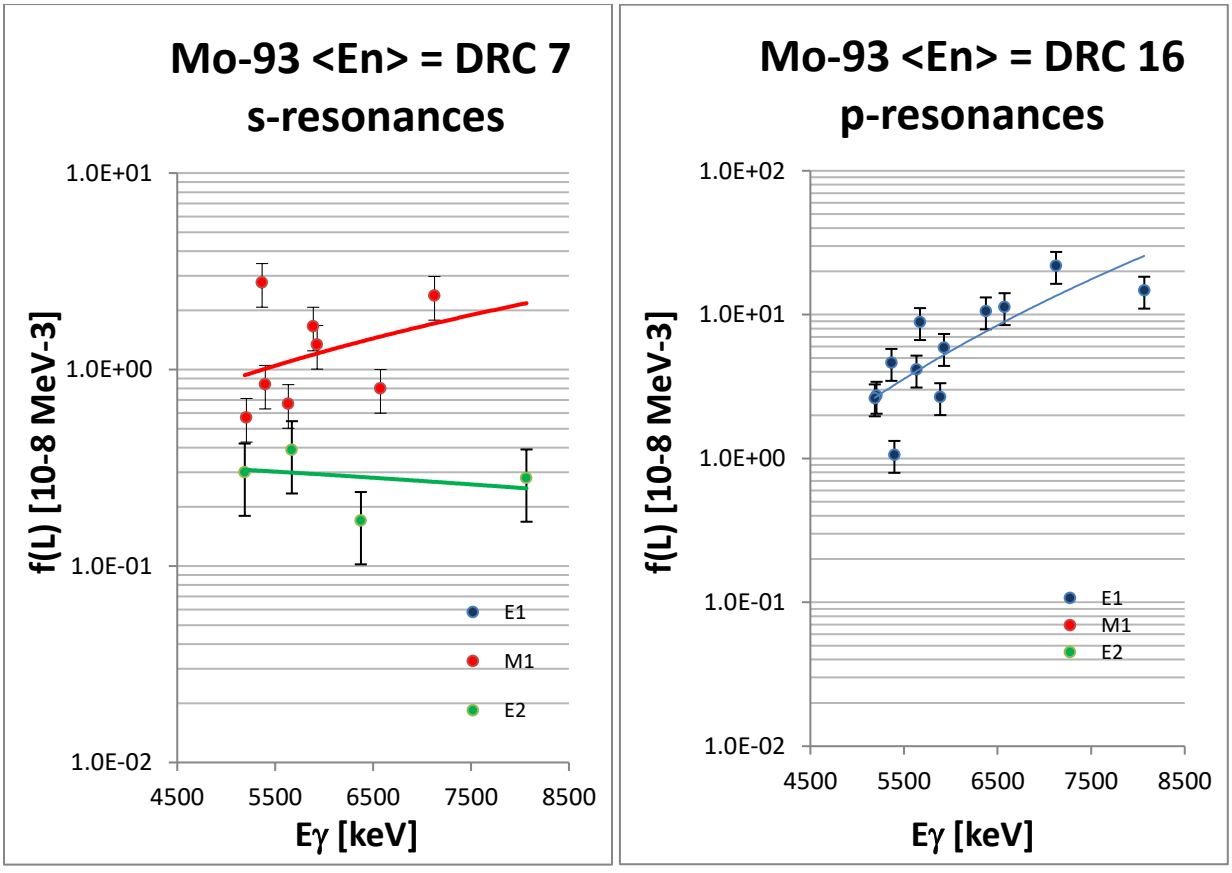

FIG. 3 *DRC Mo-93 data averaged over two sets of s- and p-resonances separately.*

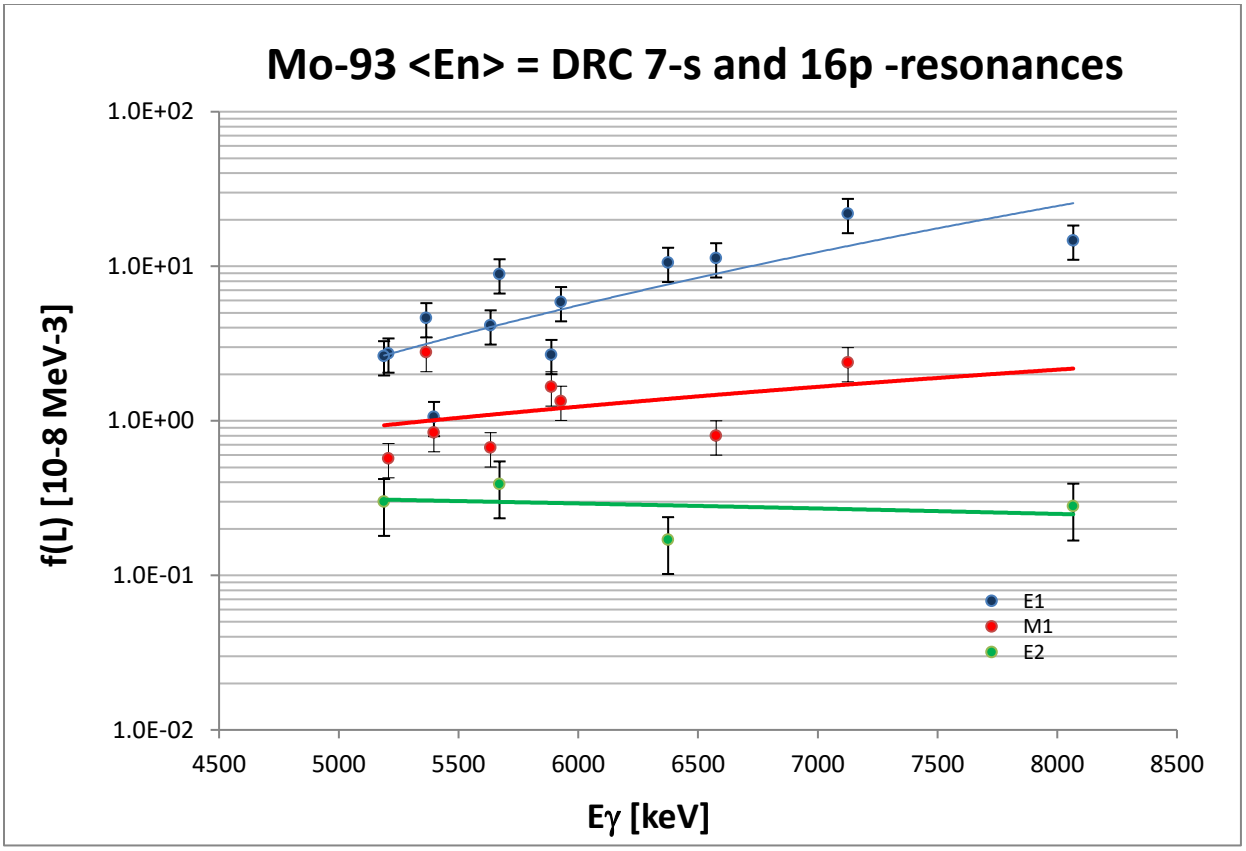

FIG. 4 *Two measurements combined in one data set with E1 and M1 transitions of the same energy originating from s- and p–wave capture. Note the rather good averaging (relatively small data dispersion) due to averaging over 23 resonances.*

Another complication in the interpretation of DRC results can come from the non-statistical mechanism in the reaction channel, which may influence the transition strength. This typically happens in low A nuclides and may dominate over the statistical nature of the capture process. This effect has been reported in several experiments, such as ^{36}Cl, ^{53}Cr or ^{57}Fe p-wave capture [16-18]. In these measurements there is a strong positive correlation between thermal and resonance capture intensities and/or spectroscopic factors and an explanation by the one-step particle transfer or two-steps valence capture via doorway states in s- and p-wave levels was proposed. In these measurements the M1 strength is often larger than the E1 strength. The use of such data to derive the systematic dependence of f(L) on the mass A can be misleading, because it may incorrectly influence the general trend of compound nucleus modeling.

3.1. Discussion of results

The data file "ATLAS DRC f(L)" includes all available DRC measurements for 57 nuclides stored in the standard E_γ, f(L), df(L), Ex and Jpi format. For the first time, DRC data were processed and compiled into a data base in a similar manner as the ARC data. Some of the DRC data have, due

to the presence of a small number of resonances, a lower accuracy, but in general many of them can form a rich complementary extension to the "ATLAS DRC f(L)" from [11]. The content of the DRC/ARC combined data base is given in Table 4.

TABLE 4 Content of the combined DRC and ARC data base

DRC - x - stems for data are processed and included in "ATLAS DRC f(L)"
ARC - 0 - data not used due to insufficient averaging or missing transition rates
ARC - x - data processed and included in "ATLAS ARC f(L)"
DRC+ARC - possible future combined f(L) data base

Product nuclide	**DRC**	**ARC**	**DRC+ARC**
F-20	x		x
Mg-25	x		x
Al-28	x		x
Si-29	x		x
Si-30	x		x
S-33	x		x
Cl-36	x		x
Sc-46	x		x
Ti-49		0	
Cr-52	x		x
Cr-54	x		x
Fe-57	x		x
Co-60	x	0	x
Cu-64	x	0	x
Cu-66		0	
Ge-74	x		x
As-76		x	x
Zr-92		x	x
Zr-93		x	x
Zr-95		0	
Nb-94	x		x
Mo-93	x	0	x
Mo-95		0	
Mo-96		x	x
Mo-97		x	x
Mo-98		x	x
Mo-99	x	0	x
Ru-100	x		x
Ru-102	x	x	x
Rh-104	x		x
Pd-106	x	x	x

Product nuclide	DRC	ARC	DRC+ARC
Ag-108		0	
Cd-114		x	x
In-116	x		x
Sb-122	x		x
Sb-124	x		x
Te-124		x	x
Te-126	x		
I-128	x	x	x
Ba-135		x	x
Ba-136	x	x	x
Ce-136		0	
Nd-144	x		x
Nd-146	x	x	x
Sm-148	x		x
Sm-150	x		x
Sm-155		x	x
Eu-154		x	x
Gd-153	x		x
Gd-155	x	x	x
Gd-156		x	x
Gd-157	x	x	x
Gd-158		x	x
Gd-159	x	x	x
Gd-161		x	x
Dy-162		x	x
Dy-163		x	x
Dy-164		x	x
Dy-165		x	x
Ho-166		x	x
Er-168	x	x	x
Er-169	x		x
Tm-170	x	x	x
Lu-176	x	x	x
Lu-177	x		
Yb-172		x	x
Yb-174	x	x	x
Hf-178	x	x	x
Ta-182	x	x	x
W-183	x		x
W-184	x	x	x
W-185		x	x
W-187		x	x

Product nuclide	DRC	ARC	DRC+ARC
Os-188		x	x
Os-189		x	x
Os-191		x	x
Os-193		x	x
Ir-192		x	x
Ir-194		x	x
Pt-195		x	x
Pt-196	x	x	x
Pt-197		x	x
Pt-199		x	x
Au-198	x	x	x
Hg-199	x		x
Hg-200	x		x
Hg-202	x		x
Th-233	x	x	x
U-235	x		x
U-236	x	x	x
U-237	x		x
U-239	x	x	x
Pu-240	x	x	x

4. Processing the quasi-mono energetic strength functions

In order to increase the statistical accuracy of DRC data, the averaged quasi-mono energetic strength function is introduced, and this has been used in all previous compilations [2-6,8]. The additional averaging is applied over a number of primary transitions in a narrow energy window to minimize the energy dependence above the phase factor. For an energy range of about 1 MeV, this is a valid assumption. The mean energy of the considered data window is usually between 6 – 7 MeV. Equation (1) can be then rewritten as

$$<<f_L\,(E_{\gamma i})>> = << \Gamma_{\gamma i} / E^3_{\gamma i} >> / D_0\ , \qquad (2)$$

where $<< \Gamma_{\gamma i} / E^3_{\gamma i} >>$ is an unweighted mean (the symbol << >> stands for the double averaging) over the used resonances and primary transitions. The advantage of this approach is that the data can be used either for a direct calibration of averaged ARC measurements or for derivation of <f(L)> systematics as a function of the mass A.

Data for each nuclide from Table 1 have been inspected and E1 and M1 transitions selected for the averaging of binned gamma transitions with the mean energy $<E_{\gamma i}>$. Following Eq. (2), only the phase factor reduction is applied and no additional energy dependency is assumed, which is

appropriate if the energy region is sufficiently narrow. An inspection of these data shows that for the majority of f(E1) and f(M1) values the $<E_\gamma>$ value does not deviate too much from the 6 – 7 MeV energy range (see Fig. 5).

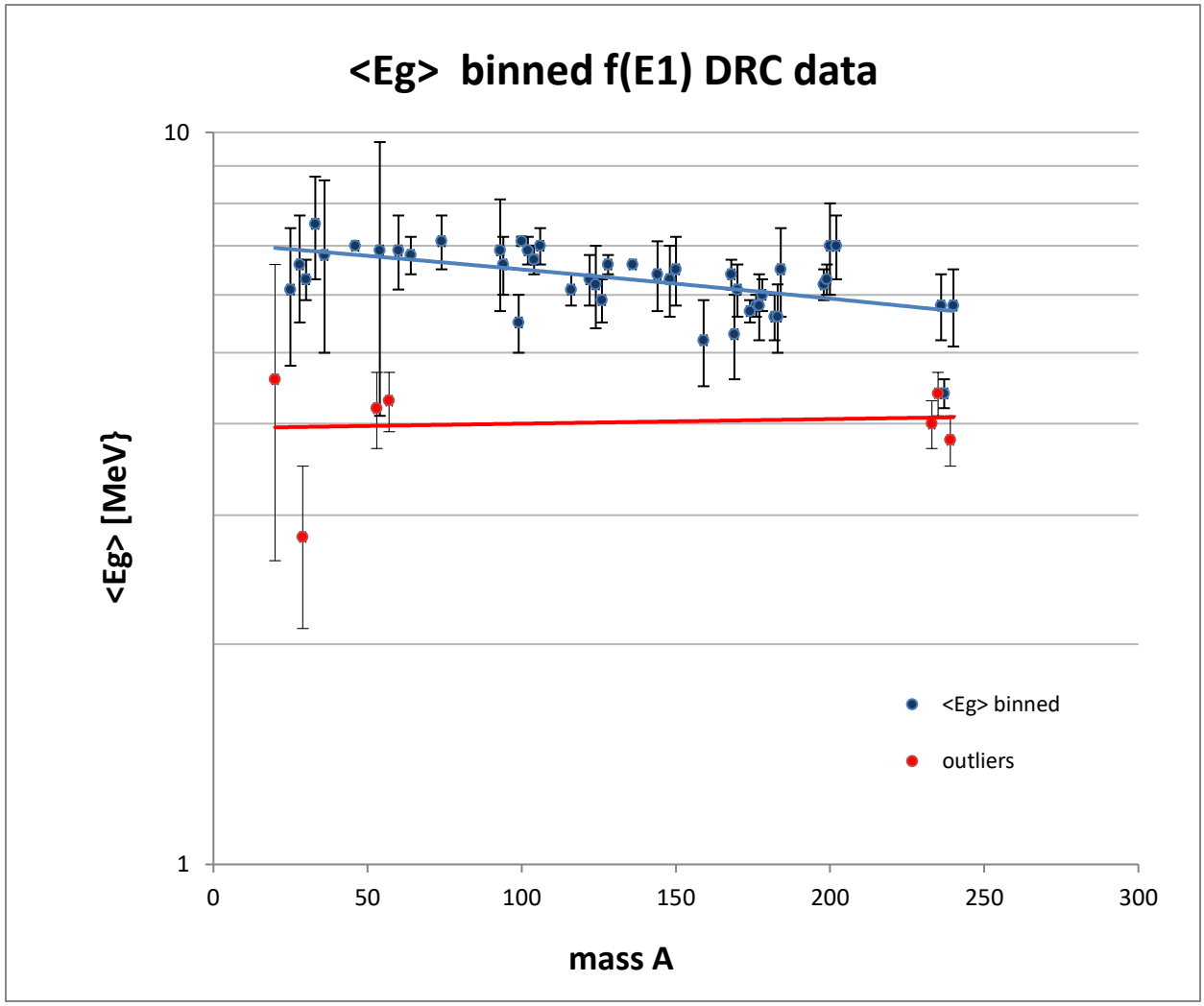

FIG. 5 *The mean energy $<E_\gamma>$ used in the derivation of $<<f(E1)>>$ values; the window width is plotted as an error bar. The red data points show nuclides which significantly differ from the main trend 6 – 7 MeV.*

Data significantly outside this region, such as ^{20}F and/or the actinides, may deviate from the general trend dependence and are discussed later. The energy correction due to the additional energy dependence $(E_\gamma/< E_\gamma>)^2$ may be considered.

Results of the analysis are shown in Table 4. The relevant parameters used are given, each nuclide has two lines, the upper one includes results from [8], printed in small font, and the lower one the present results. The number of resonances and gamma-rays used in the evaluation indicates the

degree of averaging. The mean value of $<E_\gamma>$ for the adopted data is $<E_\gamma>$ = 6.0 MeV for both E1 and M1 multipolarities.

TABLE 5 Evaluation of the quasi-mono energetic strength function f(L)

#res - number of included resonances with their l_n assignment
E1, M1 - number of selected E1 and M1 transitions for the averaging
Spacing -spacing used for the evaluation in Eq. (2)
D_0^J $D1^J$- estimated spin dependent value of the spacing D_0 and D1for the spin J
<f(L)/d(L)> - the average PSF value with the uncertainty

Nuclide	# res	E1	M1	Spacing	<f(E1) (d<f(E1)>)	<Eg>/Δ	<f(M1) (d<f(M1)>)	<Eg>/Δ
				eV	*10^{-8} MeV^{-3}	MeV	*10^{-8} MeV^{-3}	MeV
F-20	*2(p)*	*5*	*3*	*D1=33200*	*1.8(11)*	*4.4*	*4.26(310)*	*4.4*
	2(p)	7	3	D1=60000	0.63(20)	4.6/2.0	2.41(23)	5.0/0.3
Mg-25	*1(p)*	*4*		*D1=158000*	*4.68(344)*	*6*		
	1(p)	4		$D1^{3/2}$=237000	2.21(30)	6.1/1.3		
	1(d)		4	$D2^{3/2}$=220000			0.16(3)	6.1/1.3
Al-28	*2(s)*	*5*	*2*	*D0=53700*	*0.55(34)*	*6.6*	*0.77(51)*	*6.9*
	1(s) 1(p)	4	 2	$D0^3$=90630 $D1^3$=97412	0.11(3)	6.6/1.1	 0.38(9)	 7.2/0.5
Si-29	*2(p,d)*	*5*	*2*	*D0=332200*	*0.03(2)*	*6*	*0.02(1)*	*5.4*
	1(p)							
	1(d)	2	4	$D2^{5/2}$=136800	0.35(10)	2.8/0.7	0.30(3)	7.4/1.3
Si-30	*1(p)*	*2*		*D1=52400*	*1.09(75)*	*6.9*		
	1(p)	2		$D1^2$=94320	2.59(56)	6.3/0.4		
S-33	*1(p)*	*4*	*3*	*D0=179000*	*0.17(12)*	*7.5*	*7.5(8)*	*????*
	1(p)	3	3	$D1^{3/2}$=138900	0.33(3)	7.5/1.2	0.71(13)	4.2/1.2
Cl-36	*1(p)*	*9*	*5*	*D0=22300*	*0.14(7)*	*7.2*	*0.33(20*	*5.4*
	1(p)	9	5	$D1^2$=192000	0.45(7)	6.8/1.8	0.83(6)	5.6/1.0

Nuclide	# res	E1	M1	Spacing	<f(E1) (d<f(E1)>)	<Eg>/Δ	<f(M1) (d<f(M1)>)	<Eg>/Δ
Sc-46	*2(s)*	*13*	*9*	*D0=1030*	*2.03(74)*	*7*	*1.48(75)*	*7.2*
	2(s)	12	5	D0=1030	0.46(10)	7	0.63(20)	7.2
Cr-53								
	1(p)	2	8	$D1^{3/2}$=15750	5.44 (167)	4.2/0.5	1.53(13)	6.3/1.6
Cr-54	*23(sp)*	*33*	*31*	*D0=5960?*	*2.07(24)*	*6.7*	*0.70(7)*	*6.7*
	8(s)	15	31	D0=7100	9.80(150)	6.9/2.8	0.59(7)	6.7/2.3
	15(p)	5		D1=2200	6.90(170)	5.9/0.8		
	s+p	20			8.35(160)	6.9/2.8		
Fe-57								
	1(p)	3	17	$D1^{1/2}$=23100	0.17(9)	4.3/0.4	0.48(10)	5.5/2.2
Fe-59								
	2(p)		8	D1=5030			0.33(13)	5.4/1.2
Co-60	*1(s)*	*8*		*D0=1390*	*2.06(111)*	*7*		
	1(s)	8		$D0^4$=3128	2.45(60)	6.9/0.8		
Cu-64	*3(s)*	*9*		*D0=722*	*1.33(34)*	*7.5*		
	4(s)	10	2?	D0=700	2.72(68)	6.8/0.4	4.08(102)	6.3/0.1
Ge-74	*5(s)*	*7*	*7*	*D0=64???*	*2.64(90)*	*7.1*	*2.05(70)*	*7.9*
	6(s)	5	6	D0=99	5.65(140)	7.1/0.6	2.17(55)	7.6/1.1
Nb-94	*7(sp)*	*15*	*16*	*D0=84.8*	*2.24(55)*	*6.5*	*0.53(13)*	*6.5*
	3(s)		14	D0=84.8			0.15(3)	6.6/0.6
	4(p)	16		D1=50	4.96(124)	6.6/0.6		
Mo-93	*8(s)??*	*10*		*D0=970??*	*1.91(36)*	*5.5*	*0.26(4)*	*5.5*
	7(s)		8	D0=2700			1.38(35)	6.4/0.7
	16(p)	10		D1=780	7.36 (220)	6.9/1.2		
Mo-99	*17(sp)*	*7*	*8*	*D0=970*	*1.91(36)*	*5.5*	*0.26(5)*	*5.5*
	6(s)		8	D0=970			0.44(11)	5.5/0.5
	11(p)	9		D1=286	6.28(159)	5.5/0.5		

Nuclide	# res	E1	M1	Spacing	<f(E1) (d<f(E1)>)	<Eg>/Δ	<f(M1) (d<f(M1)>)	<Eg>/Δ
Ru-100	*4(s)*	*5*	*10*	*D0=21.7*	*4.3(6)*	*6.9*	*3.07(171)*	*7.4*
	4(s)	4	8	D0=21.3	8.48(212)	7.1/0.1	2.42(0.73)	7.2/0.4
Ru-102	*6(s)*		*5*	*D0=18.5*			*5.32(213)*	*7.8*
	6(s)	4	7	D0=18	21.7(54)	6.9/0.3	10.5(26)	7.1/0.5
Rh-104	*6(s)*	*4*	*2*	*D0=24.2*	*3.96(32)*	*6.9*	*0.52(31)*	*6.9*
	7(s)	10	9	D0=32	4.72(118)	6.7/0.3	1.31(39)	6.8/0.2
Pd-106	*8(s)*	*10*	*12*	*D0=10.9*	*4.14(95)*	*7.9*	*1.3(3)*	*7.9*
	9(s)	10	10	D0=10.9	3.87 (39)	7.0/0.4	0.91(28)	8.1/0.9
Ag-108	*na*	*na*	*na*	*na*	*2.19(35)*	*6.7/0.6*	*0.32(5)*	*6.7/0.6*
In-116	*31(s)*	*12*	*12*	*D0=9*	*5.87(168)*	*5.9*	*1.19(32)*	*6.1*
	23(s)	8	9	D0=9	11.9(30)	6.1/0.3	0.91(23)	6.1/0.2
Sb-122	*12(s)*	*9*	*9*	*D0=10*	*4.12(82)*	*6.1*	*0.82(16)*	*5.9*
	12(s)	10	7	D0=10	12.3(31)	6.3/0.5	1.64(46)	6.3/0.5
Sb-124	*4(s)*	*11*	*13*	*D0=24*	*3.0(2)*	*5.6*	*0.71(18)*	*5.8*
	4(s)	8	6	D0=24	4.79(126)	6.2/0.2	0.8(2)	6.3/0.2
Te-126	*6(s)*		*10*	*D0=42.7*			*1.4(3)*	*7.7*
	6(s)	8	16	D0=42.7	6.83(167)	5.9/0.4	1.32(46)	5.9/0.5
I-128	*8(s)*	*7*	*12*	*D0=9.7*	*1.9(5)*	*6.5*	*0.31(5)*	*6.5*
	8(s)	6	10	D0=9.7	8.54(256)	6.6/0.2	1.08(38)	6.6/0.3
Ba-136	*6(s)*	*1*	*4*	*D0=40*	*5.0(3)*	*6.6*	*1.67(84)*	*7.9*
	10(s)	1	7	D0=40	6.17(123)	6.6	1.10(38)	7.0/0.3
Nd-144	*10(s)*	*3*	*1*	*D0=37.6*	*5.40(22)*	*6.6*	*0.36(27)*	*6.3*
	10(s)	6	1	D0=37.6	6.17(117)	6.4/0.7	0.27(10)	6.3
Nd-146	*10(s)*	*2*		*D0=17.8*	*4.50(18)*	*6.7*		

Nuclide	# res	E1	M1	Spacing	<f(E1) (d<f(E1)>)	<Eg>/Δ	<f(M1) (d<f(M1)>)	<Eg>/Δ
					No data			
Sm-148	*12(s)*	*16*		*D0=5.7*	*4.5(9)*	*6.6*		
	23(s)	18	11	D0=5.7	4.39(117)	6.3/0.7	1.39(35)	5.3/0.3
Sm-150	*3(s)*	*13*		*D0=2.2*	*7.83(157)*	*6.5*		
	3(s)	14		D0=2.2	5.42 (136)	6.5/0.7		
Gd-153	*na*	*na*		*na*	*11.0(3)*	*na*		
					No data			
Gd-155	*15(s)*	*8*		*D0=13.8*	*8.70(18)*	*5.9*		
					No data			
Gd-157	*na*	*5*		*D0=30.5*	*12.4(223)*	*6*		
					No data			
Gd-159	*12(s)*	*8*	*9*	*D0=87*	*8.8(29)*	*5.3*	*1.5(3)*	*5.1*
	12(s)	9	8	D0=87	9.21(230)	5.2/0.7	1.22(32)	5.1/0.3
Er-168	*45(s)*	*6*	*4*	*D0=4*	*15.9(148)*	*6.4*	*4.7(5)*	*6.4*
	81(s)	10	4	D0=4	16.6(325)	6.4/0.3	4.23(102)	6.4/0.3
Er-169	*7(s)*	*6*	*9*	*D0=94*	*6.4(15)*	*4.9*	*1.6(9)*	*5.2*
	4(s)	9	1	D0=94	7.31(119)	5.3/0.7	1.56(47)	5.4
Tm-170	*9(s)*	*16*		*D0=7.28*	*4.72(101)*	*5.9*		
	10(s)	16	2	D0=7.28	6.31(126)	6.1/0.5	1.42(43)	6.0/0.2
Lu-176	*11(s)*	*8*	*2*	*D0=3.45*	*7.4(25)*	*5.8*	*3.2(14)*	*5.8*
	12(s)	8		D0=3.45	4.57(62)	5.8/0.2		
Lu-177	*6(s)*	*15*		*D0=-1.61*	*8.9(41)*	*5.9*		
	6(s)	13		$D0^{15/2}$=3.03	3.23(59)	5.8/0.6		
Y-174	*22(s)*	*5*		*D0=8.06*	*19.4(32)*	*6.3*		
	24(s)	12		D0=8.06	37.8(67)	5.7/0.2		

Nuclide	# res	E1	M1	Spacing	<f(E1) (d<f(E1)>)	<Eg>/Δ	<f(M1) (d<f(M1)>)	<Eg>/Δ
Hf-178	*37(s)*	*18*	*3*	*D0=2.4*	*18.5(35)*	*6.5*	*3.8(15)*	*6.2*
	20(s)	21	5	D0=2.32	31.7(676)	6.0/0.3	4.62(88)	6.0/0.3
Ta-182	*19(s)*	*66*	*1*	*D0=4.17*	*11.3(16)*	*5.2*	*7.17(384)*	*4.3*
	19(s)	24	5	D0=4.4	9.2(19)	5.6/0.4	1.3(3)	5.6/0.4
W-183	*7(s)*	*15*	*5*	*D0=66*	*10.7(33)*	*5.2*	*4.4(19)*	*4.7*
	7(s)	6	1	D0=63.4	10.6(26)	5.6/0.6	0.2(1)	4.9
W-184	*6(s)*	*13*		*D0=12*	*28.1(97)*	*6.3*		
	6(s)	10		D0=12	36.9(99)	6.5/0.9		
Pt-196	22(s)	9		D0=16.3	17.2(22)	7		
					No data			
Au-198	*4(s)*	*5*		*D0=15.7*	*11.4(53)*	*6.4*		
	4(s)	17	1	D0=15.7	20.0(41)	6.2/0.3	6.34(19)	5.4
Hg-199	*2(s)*	*4*		*D0105*	*55.3(253)*	*6.5*		
	2(s)	8	3	D0=105	27.8(30)	6.3/0.3	1.3(6)	5.6/0.3
Hg-200	*3(s)*	*9*		*D0=100*	*9.62(356)*	*7.2*		
	3(s)	11		D0=85	14.3(209)	7.0/1.0		
Hg-202	*3(s)*	*3*		*D0=100.5*	*8.47(693)*	*7.2*		
	3(s)	7		D0=90	33.7(80)	7.0/0.7		
Th-233	*5(s)*	*3*	*1*	*D0=18.2*	*21.1(88)*	*4.2*	*10.2(6)*	*4.5*
	5(s)	12	21	D0=18.2	33.4(836)	4.0/0.3	9.67(242)	4.2/0.3
U-235	*4(s)*	*53*	*19*	*D0=12.3*	*13.7(44)*	*3.9*	*2.4(9)*	*4.4*
	3(s)	11	8	D0=12.3	9.8(19)	4.4/0.3	2.46(11)	4.4/0.3
U-236								
	19(s)	6		D0=0.49	7.14(131)	5.8/0.6		
U-237	*7(s)*	*2*	*3*	*D0=14.7*	*8.55(369)*	*4.6*	*0.39(17)*	*4.8*
	7(s)	7	6	D0=14.7	4.45(112)	4.4/0.2	0.23(6)	4.6/0.5

Nuclide	# res	E1	M1	Spacing	<f(E1) (d<f(E1)>)	<Eg>/Δ	<f(M1) (d<f(M1)>)	<Eg>/Δ
U-239	*23(s)*	*9*	*5*	*D0=16.4*	*10.29(254)*	*3.8*	*2.6(8)*	*4.4*
	23(s)	10	5	D0=16.4	7.70(173)	3.8/0.3	2.10(57)	4.2/0.6
Pu-240								
	7(s)	5	2	$D0^1$ = 2.73	18.0(48)	5.8/0.7	2.68(67)	6.1/0.4

The given uncertainties for binned transitions include the average statistical errors of $<I_{\gamma i}>$ or $<\Gamma_{\gamma i}>$ taken from the original references. The Porter-Thomas fluctuation has not been included in the quoted errors, which depends on the number of isolated resonances υ and may be estimated by the expression $\sqrt{(2/\upsilon)}$. Another quantity which may influence the calculation of <<f(L)>> is the uncertainty in the resonance spacing. In several critical reviews some significant disagreements were spotted, and these may introduce an additional uncertainty to the evaluated strength functions. The errors of the spacing D are not included in the evaluated f(L) uncertainty, but the D values used in two last evaluations are given in Table 5 for a comparison.

4.1. Discussion of results

All surveyed data with their newly analyzed <<f(L)>> values are displayed in Figs. 6 and 8 as a function of the mass number A. The dotted lines represent one standard deviation (SD) uncertainty (68% confidence limit) to give an impression of the size of fluctuations.

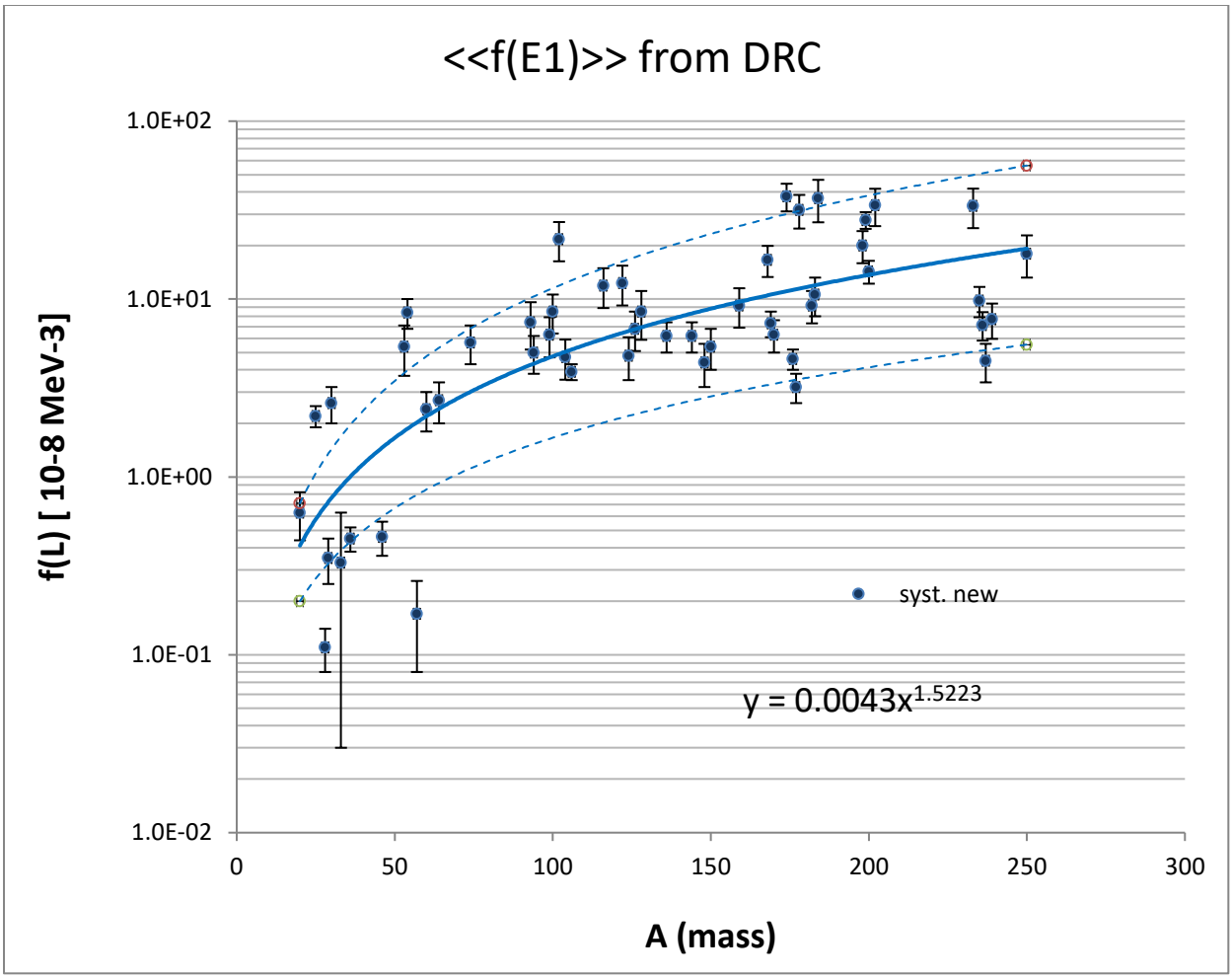

FIG. 6 *Quasi-mono energetic doubly average strength functions <<f(E1)>> from the present analysis with trend curve systematic as a function of the mass A. The dotted line is one SD dispersion from the LSQ procedure.*

The LSQ fit using a power function of the mass number A results in an expression of the strength functions systematics E1 and M1 shown in Eq. (4)

$$\mathbf{<<f(E1)>> = 0.004\ A^{1.52\pm0.21}\ and\ <<f(M1)>> = 0.12\ A^{0.49\pm0.10}},\qquad (4)$$

where $R^2 = 0.6$ and $R^2 = 0.13$. R^2 is a measure of the goodness of the fit of the trend line to the data. The quoted uncertainties are 1 SD errors from the LSQ fit further increased by Γ_γ and D uncertainty estimates of 10%.

The E1 data follow reasonably the expected smooth trend (see Fig. 6) with two exceptions, the mass regions with A < 50 and 170 < A < 190. The major outliers for light nuclides are now shown in detail in Fig. 7. The basic feature of these nuclides is that only one or two resonances are used (often p-wave capture) and the applied spacing has to reflect the spin dependence (see ^{25}Mg, ^{28}Al, ^{29}Si, ^{30}Si, ^{36}Cl, ^{53}Cr, ^{57}Fe and ^{60}Co nuclides). The D(J) estimates were determined from the (2J+1)

dependence of the level density, in case the spin of the resonance is unknown, the D_0 or D_1 values were used.

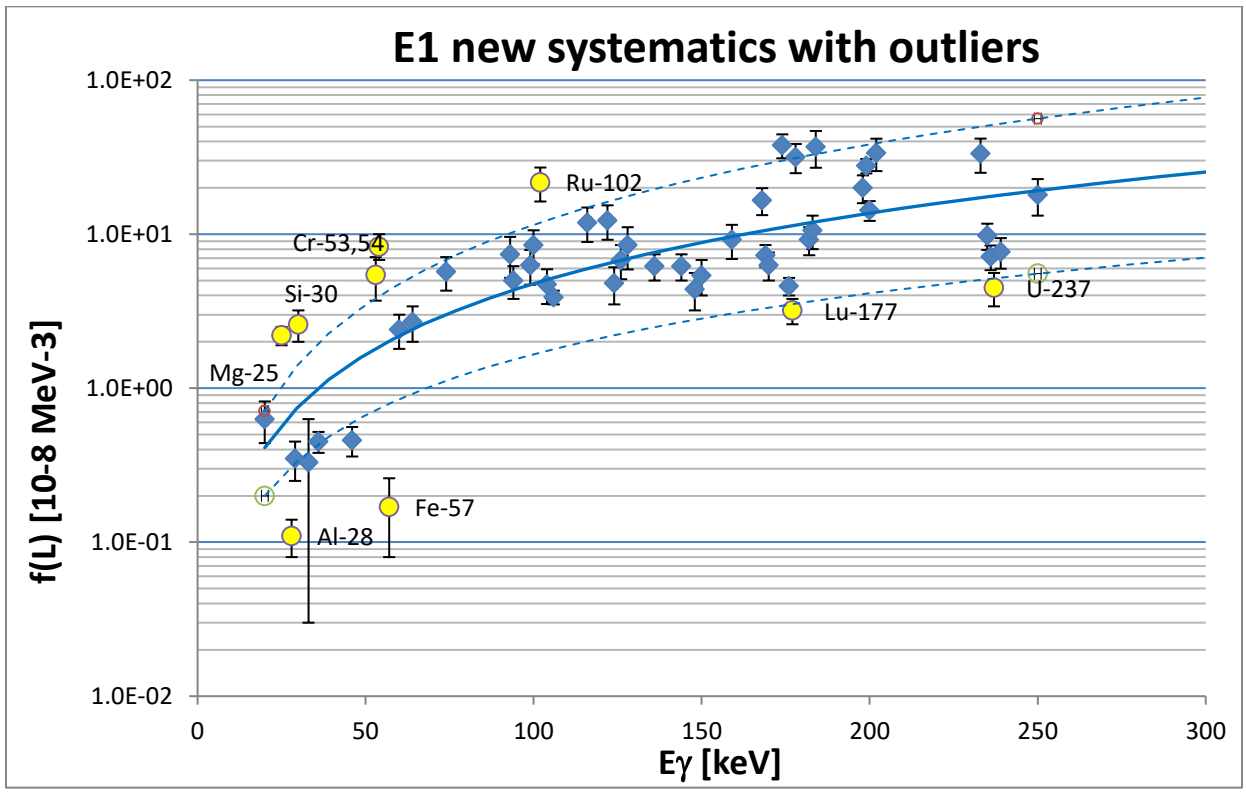

***FIG.** 7 Major outliers of the doubly average <<f(E1)>> strength function systematic. The major outliers (yellow data pints) are discussed in Table 6.*

Furthermore, the non-statistical character of some of the primary transitions may be contributing. As discussed in Section 3, the valence capture via doorway states in s- and p-wave levels means that M1 strength is larger than the E1 strength. This may explain why these data points fall below the average trend.

The scatter in the $170 < A < 190$ region is more complex and is greatly influenced by 3 major outliers, the measurements for ^{174}Yb, ^{184}W and ^{202}Hg. One explanation may be that they belong to deformed nuclides (see also other entries in $160 < A < 190$ region), with an increased gamma strength, as shown by Kopecky, Uhl and Chrien [19] and for which an empirical enhancement factor has therefore been introduced in the EGLO model. In addition, a strong overestimation of the trend line was found for the ^{102}Ru nuclide, both for E1 and M1 radiation. There is no explanation available for this nuclide.

The situation for M1 radiation is complicated for several reasons. The systematic trend of the M1 strength function (see Fig. 8) shows a similar mass dependence as the E1 case. However, the data fluctuation is broader, which may point to larger inaccuracies of M1 compared to E1 data. Possible reasons may be less statistical accuracy, inadequate averaging, etc. To address this situation, the

two SD criteria have been used to identify the outliers. The most probable theoretical model for M1 transition strength above 5 MeV is a standard Lorentzian based on the spin-flip resonance and the Brink hypothesis. In such a case the presented data are close to the resonance maximum or its tail at lower energies.

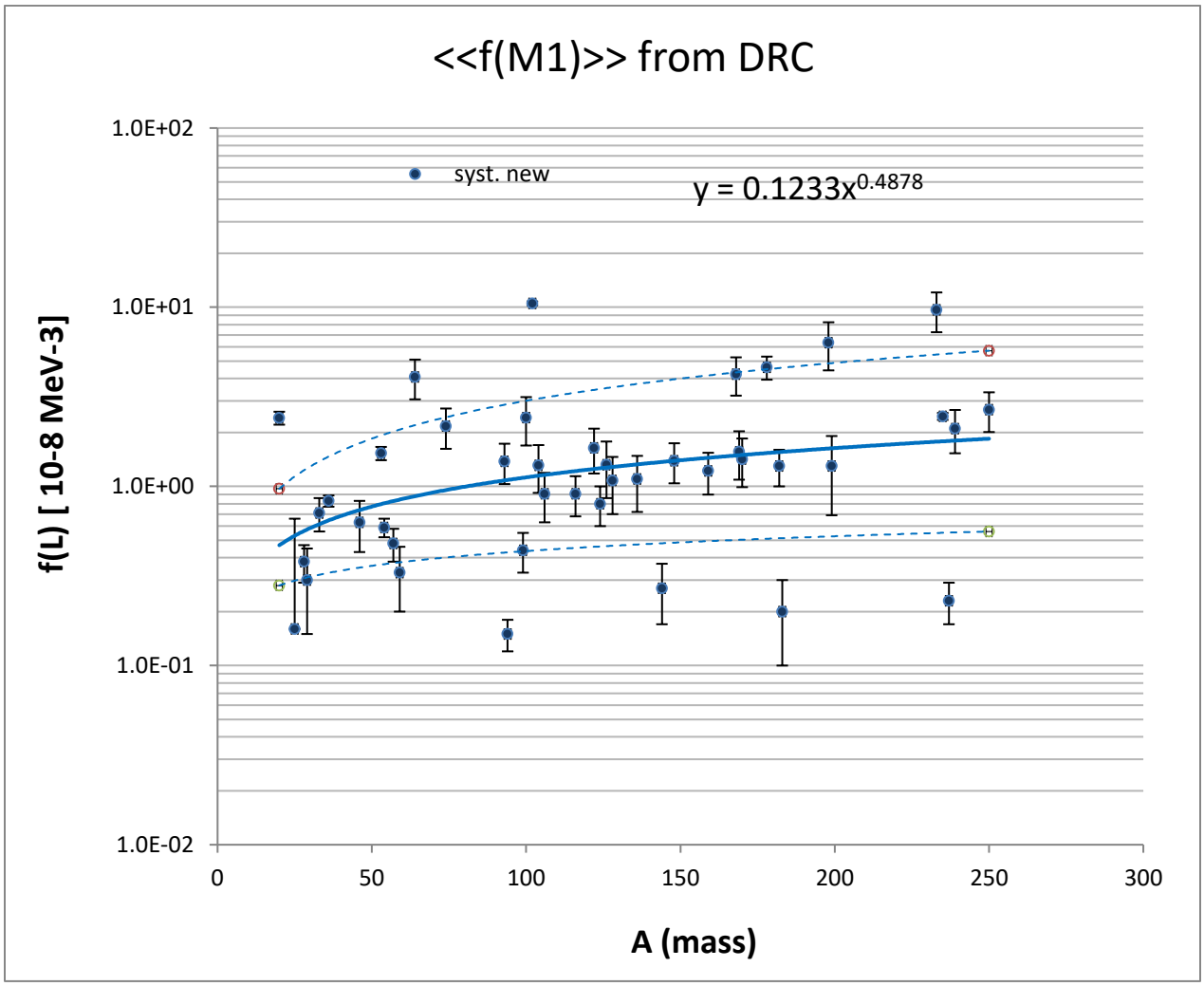

FIG. 8 *Quasi-mono energetic doubly average strength functions <<f(M1)>> from the present analysis with trend curve systematic as a function of the mass A. The dotted line is two SD dispersion from the LSQ procedure.*

The major outliers are shown in Fig. 9. The strongly enhanced point of ^{102}Ru nuclide is discussed above in the E1 section. Three strongly underestimated data points above A = 150 belong to ^{144}Nd, ^{183}W and ^{237}U, with only one M1 transition and therefore the uncertainty is very large. Some of the enhanced data between A = 150 – 200 seem to cluster again in an enhanced structure. Comments on major trend outliers are summarized for both E1 and M1 data in Table 6.

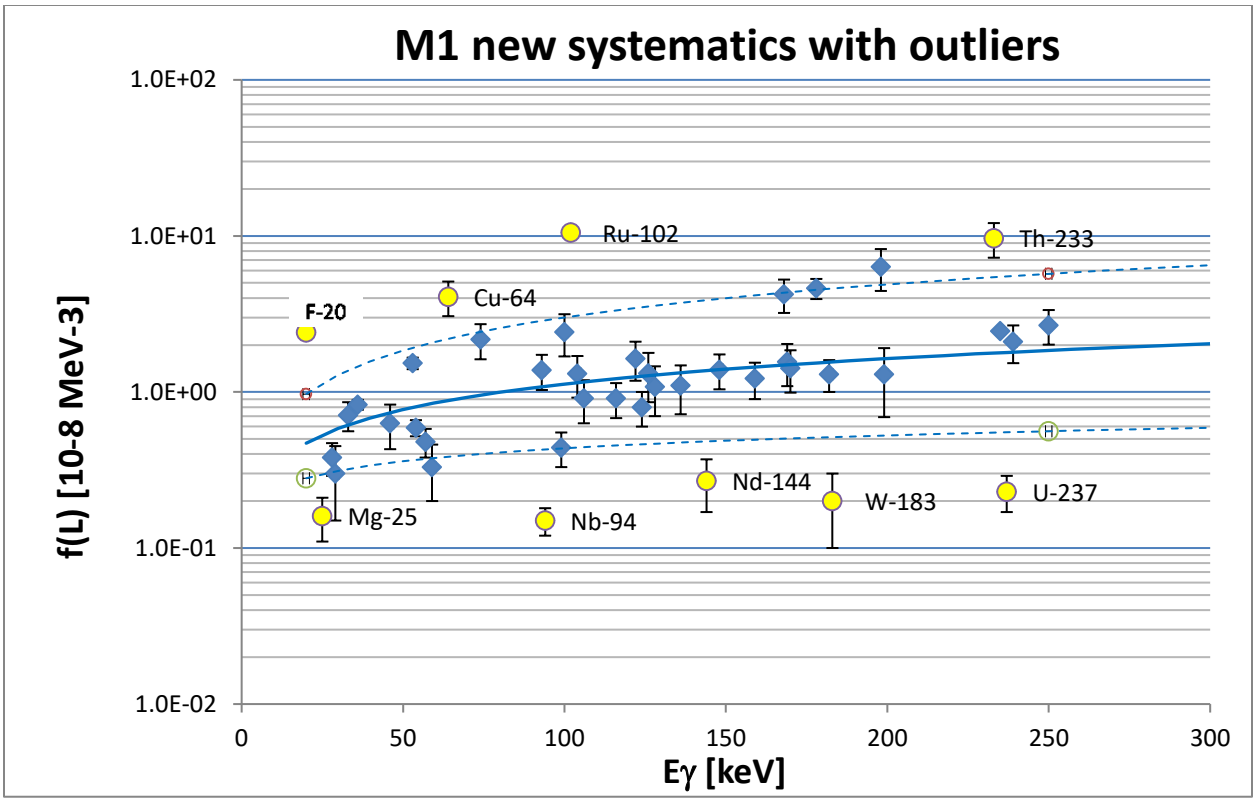

FIG. 9 *Major outliers in the doubly average <<f(M1)>> strength function systematic*

TABLE 6 Comments on outliers with possible explanations

Nuclide		**Comment**
^{20}F	M1	M1/E1 > 1 non-statistical effects
^{25}Mg	E1M1	p + d-waves, D(J) uncertainty
^{28}Al	E1	M1/E1 > 1 non-statistical effects
^{30}Si	E1	only two E1 transitions non-statistical effects D(J) uncertainty
^{53}Cr	E1	only two E1 transitions J_π final state uncertain
^{54}Cr	E1	E1s- and p-waves together; $f(E1)_i$ from ref . [8] appendix (experiment?)
^{57}Fe	E1	only three E1 transitions non-statistical effects
^{64}Cu	M1	only two M1 transitions J_π final state uncertain
^{94}Nb	M1	$\Gamma_{\gamma i}$ from ref . [14] appendix (experiment?)
^{102}Ru	E1M1	both E1 and M1 too strong, no explanation (experiment?) several extremely strong transitions
^{144}Nd	M1	only one M1 transition
^{183}W	M1	only one M1 transition J_π final state uncertain
^{233}Th	M1	both E1 and M1 too strong, no explanation (experiment?)
^{237}U	M1	both E1 and M1 too weak, no explanation (experiment?)

4.2. Comparison with previous DRC analysis

Both of the most recent evaluations in general agree (see Figs. 10 and 11), with comparable data dispersion. In the two plots the data points are shown together with the calculated trend line and in the lower part (green data points) we plot the ratio of "old/new" data scaled by 10^{-3} for E1 and 10^{-2} for M1 ratio. The reason for this comparison is that these two independently processed data may reveal and possibly verify some shortcomings in applied assignments or incorrect use of parameters.

Some further explanatory comments to the previous analysis should be mentioned. The development of the early analysis covered almost 20 years, starting from the work of McCullagh [2]. The following works mainly addressed the update of neutron resonance level spacing D and the original transition strengths from Ref. [2] were kept unchanged. The other relevant parameters, such as resonance and final state spins or the E1 and M1 assignments, remained also unchanged in Refs. [3-6,8].

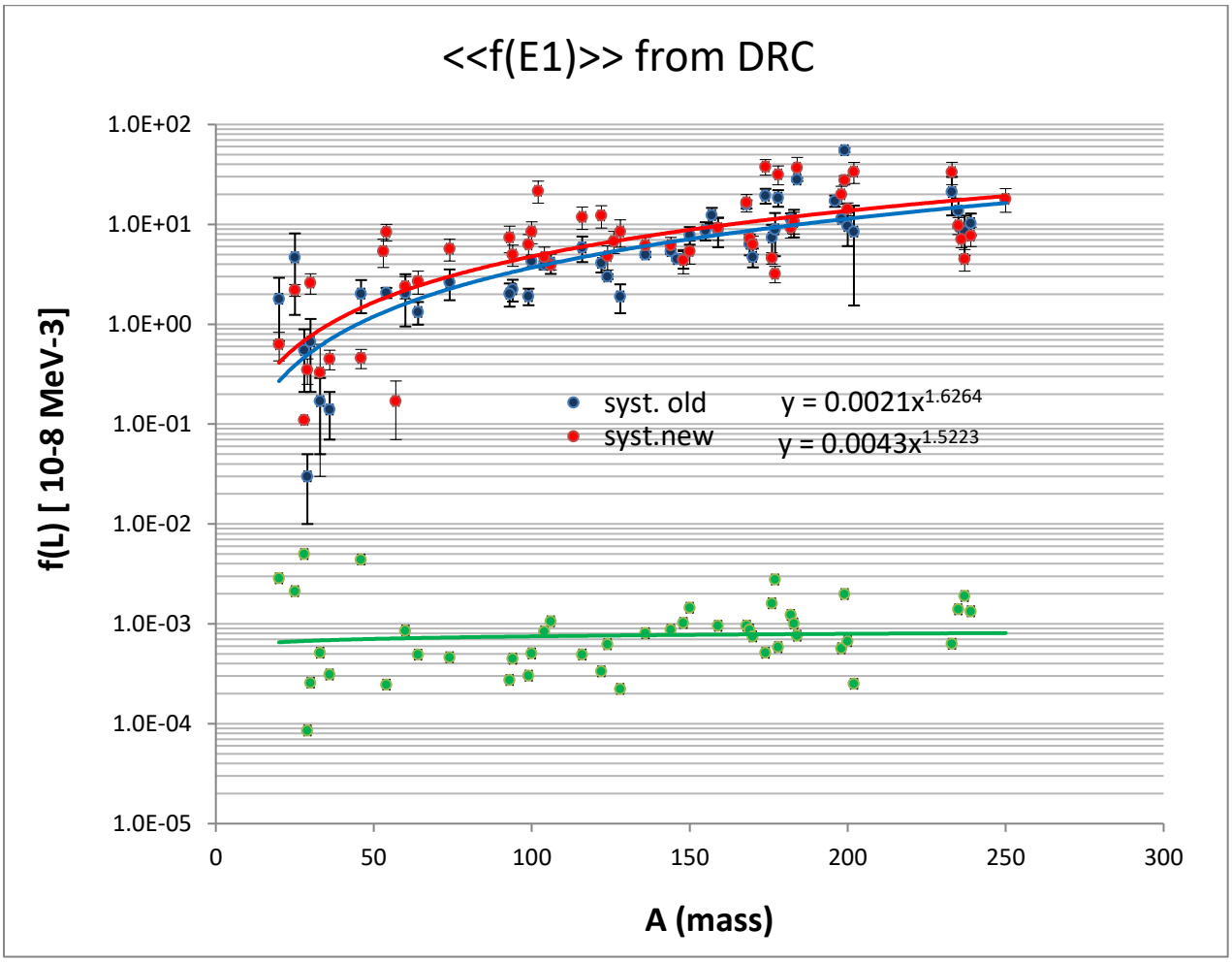

FIG. 10 *Quasi-mono energetic doubly average strength functions <<f(E1)>>from the present (new) and previous (old) analysis with trend curve systematic as a function of the mass A. Green data show the ratio of old/new systematic data point using a 10^{-3} scale.*

For M1 radiation both systematic equations give almost the same trend, while for the E1 radiation the recent systematics for nuclides with A < 100 is slightly higher. This may be due to several low mass data points in the earlier data set, which show some differences in both treatments. Another reason may come from several newly introduced assignments of E1 and M1 transitions based on the recent J_π values of final states obtained from ENSDF [10].

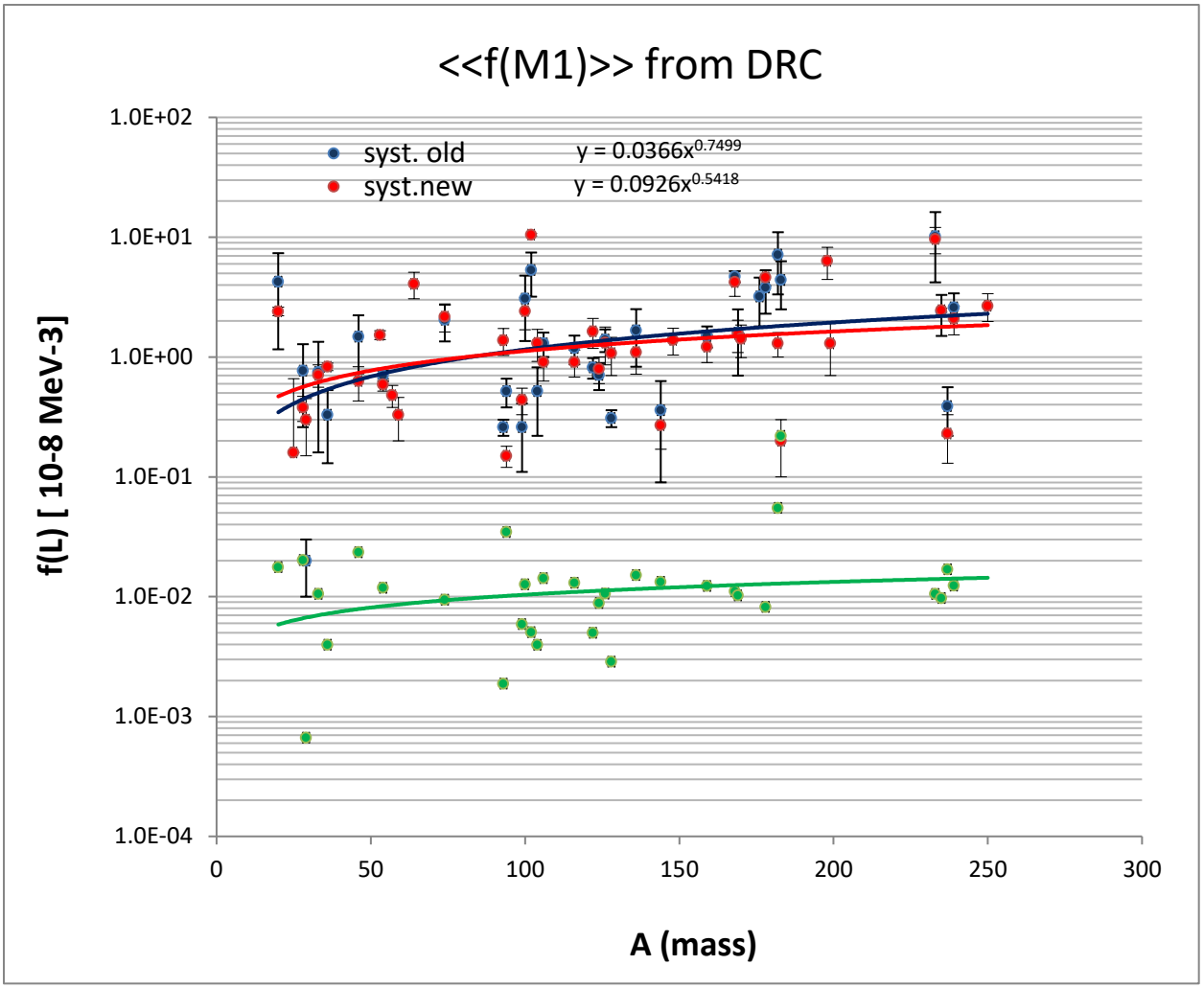

FIG. 11 *Quasi-mono energetic doubly average strength functions <<f(M1)>> from the present (new) and previous (old) analysis with trend curve systematic as a function of the mass A. Green data show the ratio of old/new systematic data point using a 10^{-2} scale.*

The ratio of both data sets in the comparison plots (green points in Figs. 10 and 11) is very close to one, which shows that despite some disagreeing entries the trend remains almost the same. However, the recent systematic trend for both E1 and M1 transitions slightly overestimates the previous data for nuclides with A < 100. This effect may be accounted for by errors or differences in the parameters used or transition assignments. In order to illustrate the comparison, ratios of <<f(L)>> old/new were plotted in Figs. 12 and 13 for E1 and M1 transitions. The major disagreements with old/new ratios that are well above a factor of two are listed in Table 7.

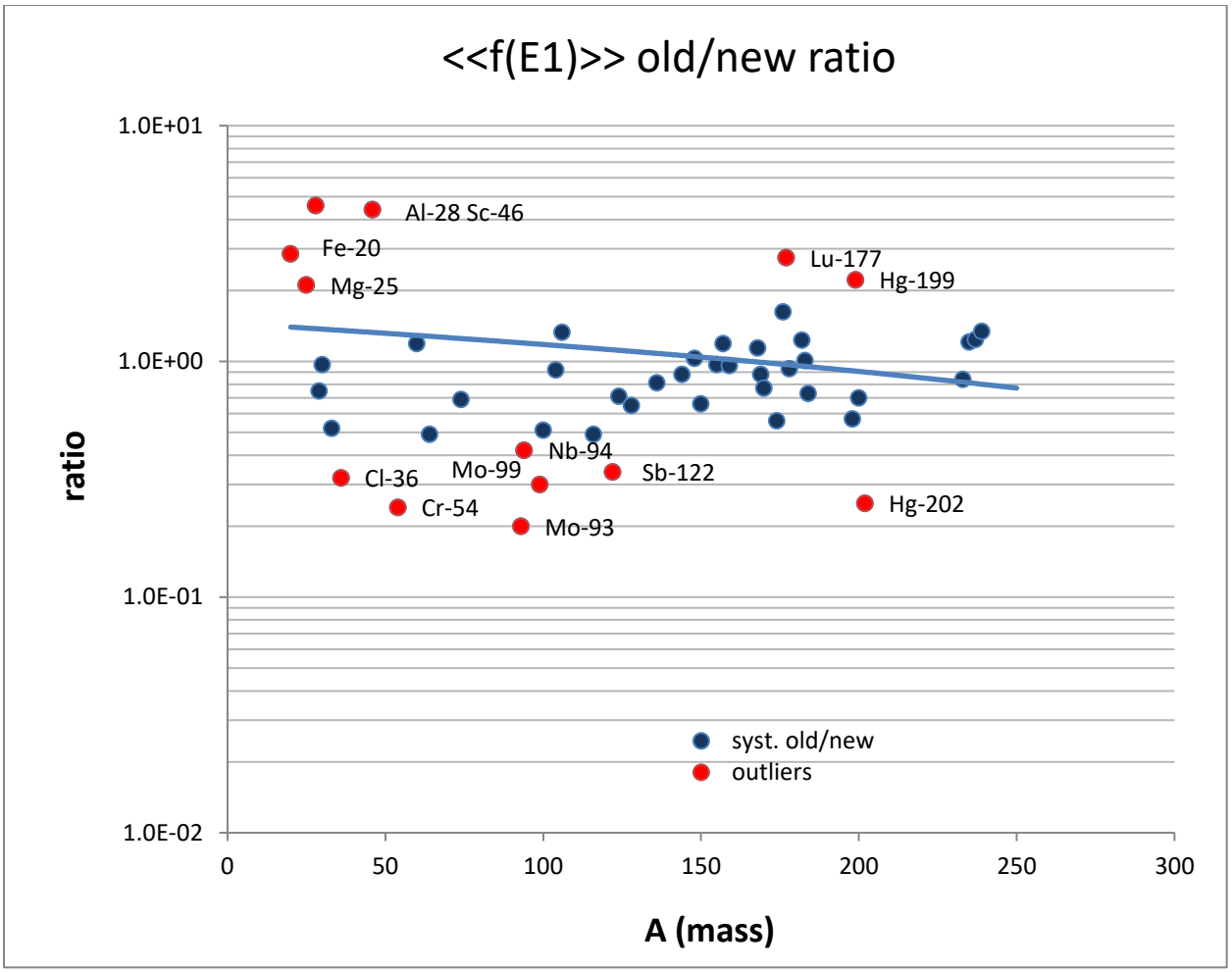

FIG.12 *Ratio of average strength functions <<f(E1)>> from previous (old) and present (new) analysis taken from Table 5. The red data points are identified outliers.*

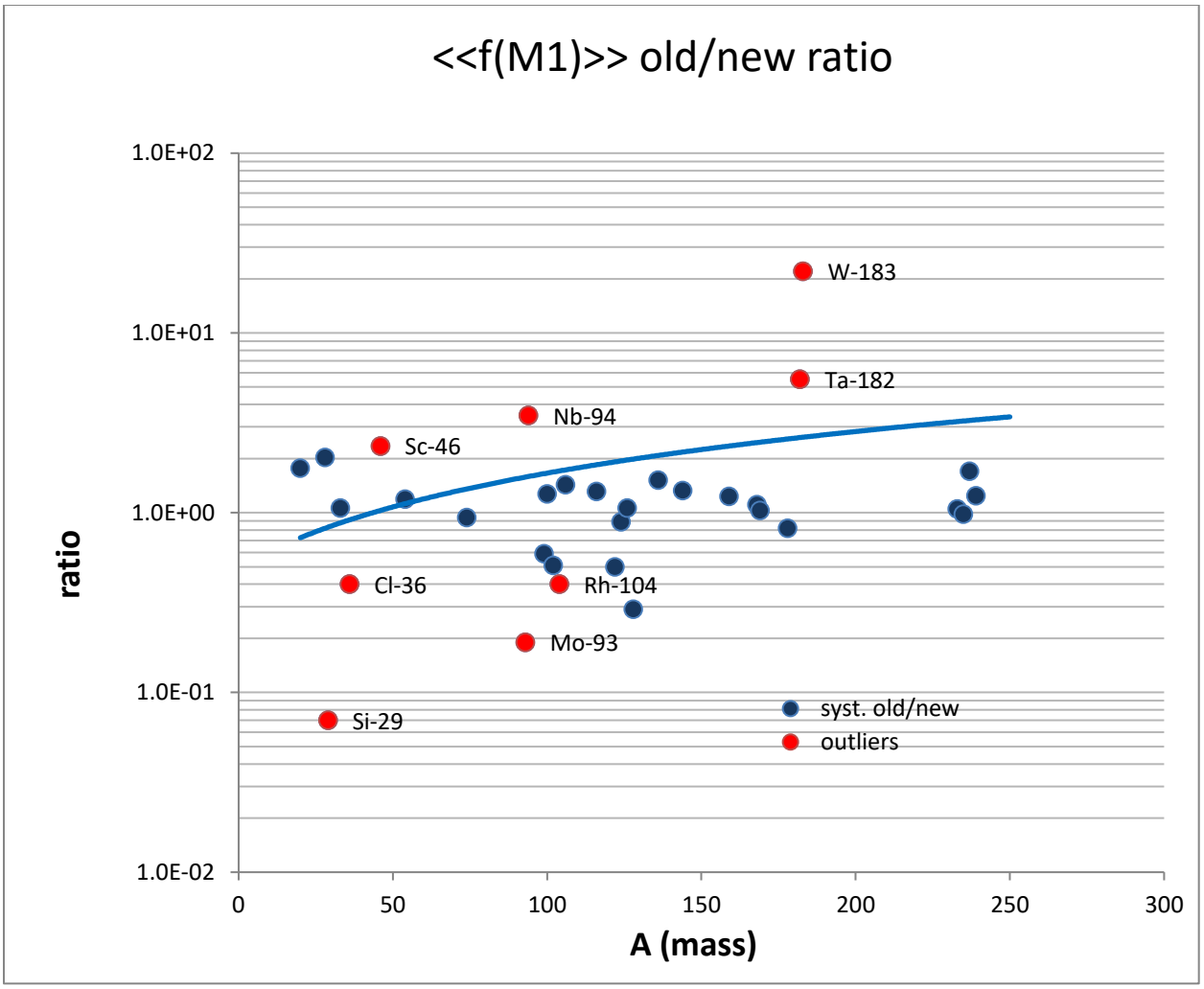

FIG. 13 *Ratio of average strength functions <<f(M1)>> from previous (old) and present (new) analysis taken from Table 5. The red data points are identified outliers.*

The possible reasons for differences between <<f(E1)>> and <<f(M1)>> values from previous and present DRC analysis are given in Table 7. They can be categorized generally in three groups: different or incorrect used spacing, differences in selected resonances and /or in used E1 and M1 transitions (their number or the multipolarity assignment).

TABLE 7 Comments on outliers with possible explanations

Nuclide		Comment
^{20}F	E1	Two rather different D_1 spacing used
^{25}Mg	E1	D(J) applied
^{28}Al	E1	Different E1 and M1 assignments
^{29}Si	M1	Incorrect D_0 used
^{36}Cl	E1M1	D(J) applied
^{46}Sc	E1M1	Difference in selected E1 and M1 transitions
^{54}Cr	E1	Incorrect D_0 used
^{94}Nb	E1M1	Difference in selected E1 and M1 transitions
^{93}Mo	E1M1	Difference in selected resonances and E1 and M1 transitions
^{99}Mo	E1M1	Difference in selected resonances and E1 and M1 transitions
^{104}Rh	M1	Difference in selected E1 and M1 transitions
^{122}Sb	E1	No explanation
^{177}Lu	E1	D(J) applied
^{182}Ta	M1	Difference in selected E1 and M1 transitions
^{183}W	M1	Difference in selected E1 and M1 transitions
^{199}Hg	E1	Difference in selected E1 and M1 transitions
^{202}Hg	E1	Difference in selected E1 and M1 transitions

4.3. Comparison with PSF model (QRPA approach)

The quasi-monoenergetic binned data have been compared with the D1M-QRPA predictions [20]. The theoretical values of f(L) have been derived from the QRPA predictions for the same E_γ-energy window as the experimental DRC binned results. This increases the sensitivity of the comparison to the energy dependence of the PSF shapes. The result for E1 and M1 strength is shown in Figs. 14 and 15.

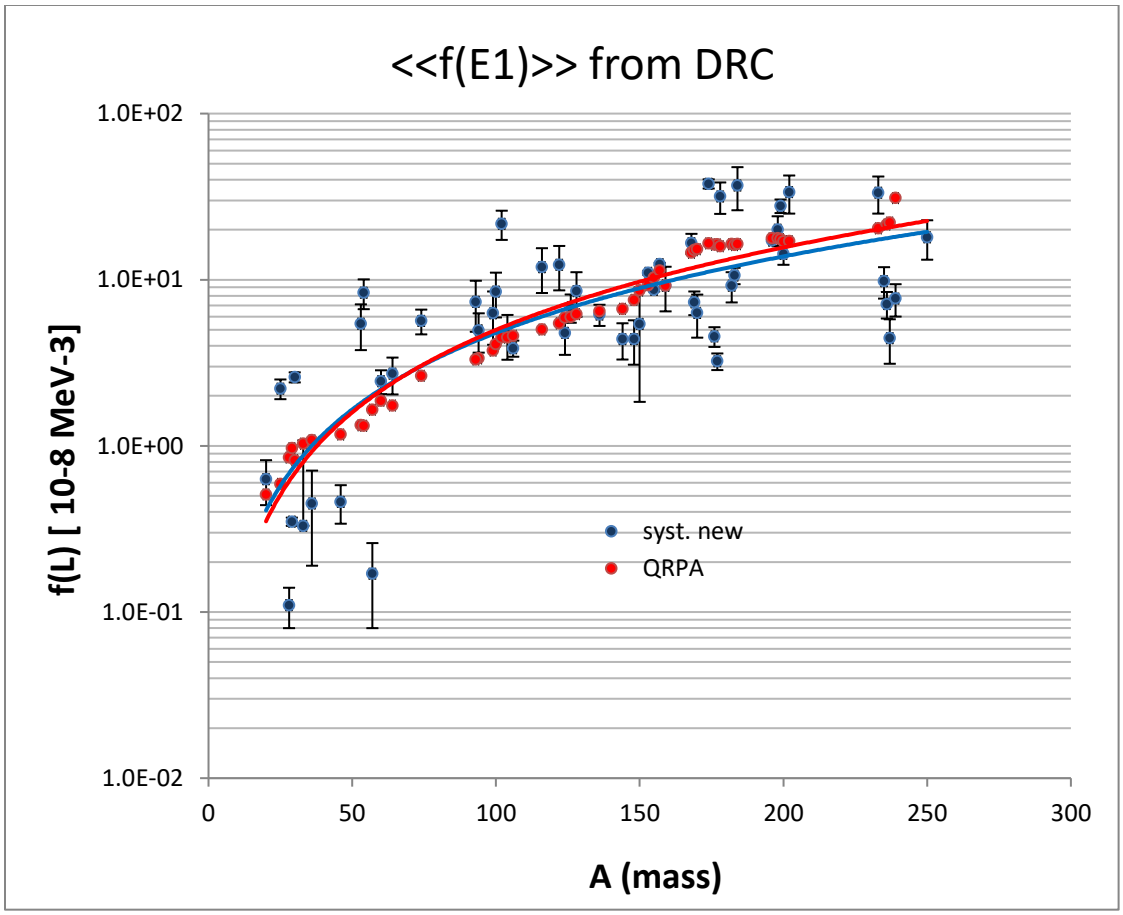

Fig. 14 *The quasi-monoenergetic <<f(E1)>> data from the DRC experiments are compared with the theoretical QRPA prediction in the same 6 – 7 MeV E_γ-energy window.*

The agreement between theoretical and experimental f(E1) values is very good and confirms the role of the E1 radiation strength as an absolute calibrator of PSF data at energies between 6 - 7 MeV. The situation for M1 is more complicated. The DRC trend curve is higher than the theoretical curve, especially for light nuclei below A < 100. This may be due to non-statistical contributions from p-wave resonances which are often present in this mass region, for which M1 is stronger than E1 radiation. Another reason may stem from the fact that the PSF obtained from microscopic calculations of different M1 excitation modes has a far more complicated form than the smooth E1 shape. Some of the outliers are a result of the poor averaging procedure over few or only one measured M1 transition. However, in this work we decided to use all measured data. For heavier nuclei with A > 100 the trend curves are in satisfactory agreement.

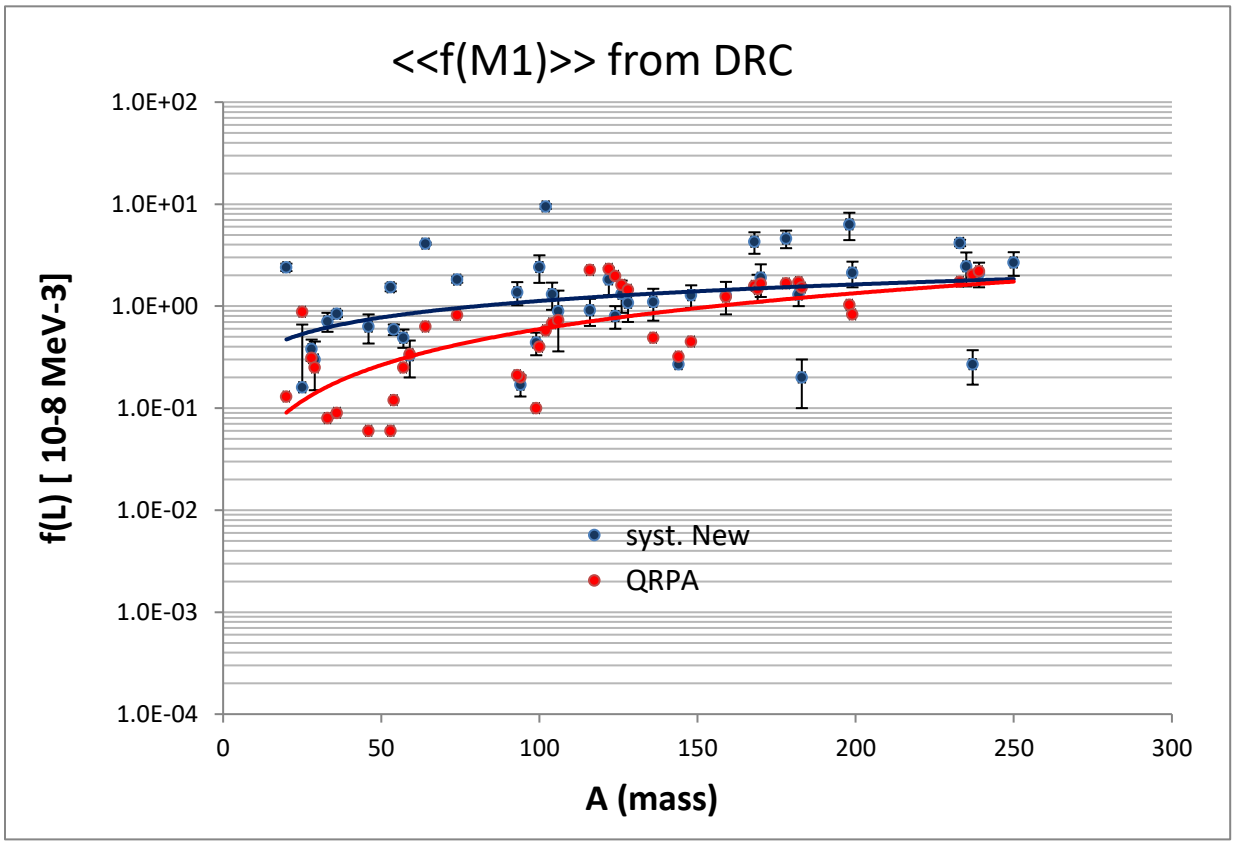

Fig. 15 *The quasi-monoenergetic <<f(M1)>> data from the DRC experiments are compared with the theoretical QRPA prediction in the same 6 – 7 MeV E□-energy window.*

5. Conclusions and recommendations

The earlier DRC measurements have been revisited and newly processed into the average strength function format, both as partial (for isolated gamma transitions - for the first time), and binned format (transitions in a gamma energy window) for 57 nuclides from ^{20}F up to ^{240} Pu. Several DRC nuclides include enough resonances and may be used to form a new extended and comprehensive data base of PSF using combined data from both DRC and ARC measurements. This action is recommended for future work, the possible content of such a data base is shown in Chapter 2. The present results are included in the data base called *ATLAS f(L) DRC* using Excel spreadsheets.

5.1. The absolute calibration of the E1 strength

The importance of DRC data and the proper analysis of these data is twofold: they can be used to provide new PSF data but also as a tool for absolute normalization of the ARC data. The comparison of the quasi-mono energetic strength function data of the present and previous analysis from [8] showed a very good agreement of the systematic trend equations $<<f(E1)>> = 0.004A^{1.52}$ and $<<f(E1)>> = 0.002A^{1.63}$, respectively. This result demonstrates that even though some data in these two data sets differ, the final data dispersion trend is almost the same. Even older data from 1994 [3] are in satisfactory agreement with the trend (see Fig. 16).

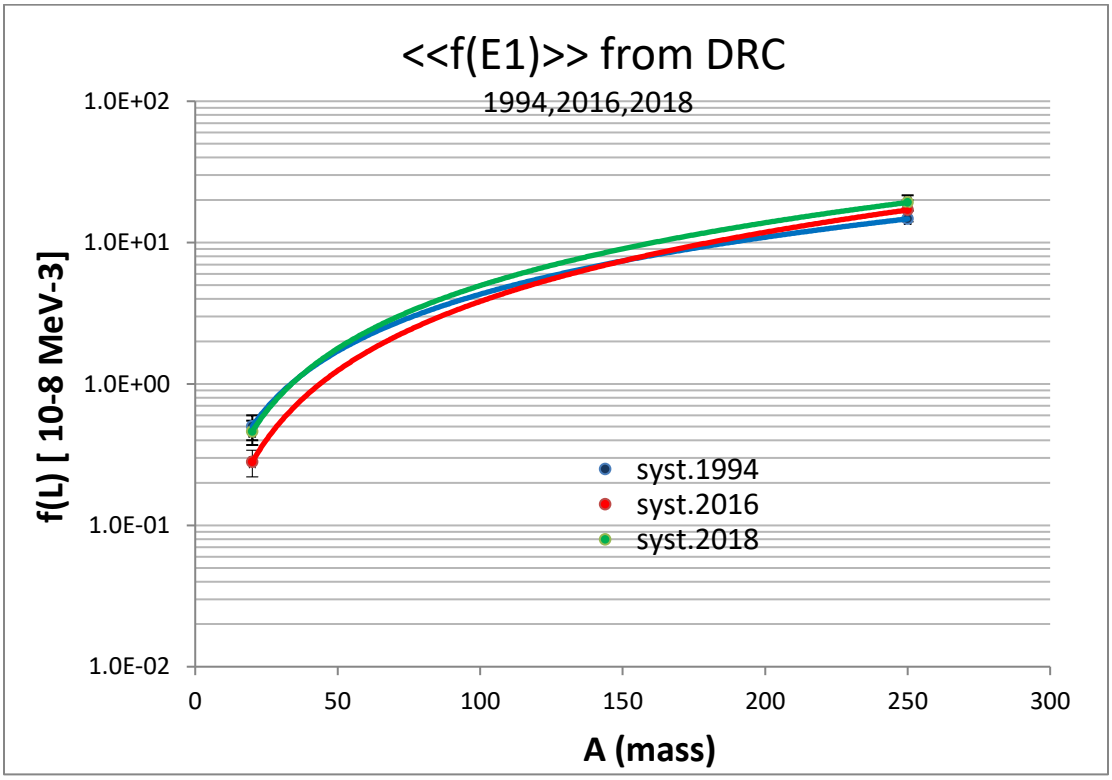

FIG. 16 *Comparison of << f(E1)>> trend systematic from Refs. [3,8] and the present work*

The majority of data lie between 6 – 7 MeV, except for the low mass and actinide nuclides. Therefore, we may conclude that the average E1 strength at the excitation of 6 – 7 MeV excitation can be given by the equation

$$\mathbf{<<f(E1)>> = 0.004A^{1.52}},$$

and can be used as an absolute normalization of experimental results or theoretical predictions. Because the M1 strength is always present in such studies, the calibration of the M1 strength may be related to the absolute E1 strength.

The dispersion of the doubly average <<f(E1)>> strength function data in Fig. 7 comes primarily from the Porter-Thomas fluctuations (insufficient averaging), the statistical uncertainty of the gamma-ray analysis, the mass dependence of the f(E1) model above the $E\gamma^2$ factor from the tail of the GDR, but also from the uncertainty in the absolute detector efficiency standards used to convert the relative gamma-ray intensity into absolute scale per captured neutron or partial radiative width. To renormalize the data in the literature with the most recent standards is an action beyond the scope of this work. Furthermore, to extract the original experimental data from some older references is not possible. These arguments support the conclusion that the systematics of <<f(E1)>> is most probably the best absolute E1 strength information.

5.2. Recommendation

The E1 systematics has been successfully applied for absolute normalization of the *ATLAS f (L) ARC* data base [11] for nuclides without corresponding DRC measurements. The agreement between systematics from 2016 and 2018 supports the normalization used in [11] and no other action is needed. It seems therefore that for a new normalization of the future *ATLAS f (L) ARC+DRC* the present results can be recommended.

Finally, the use of quasi-mono energetic strength function data for the normalization of the corresponding ARC data was also assessed (see Sect. 4.1). The good overall performance of the systematics suggests that Equation (4) chould be generally applied for all nuclides. Some more testing of this procedure is recommended in the future.

Acknowledgment

The author acknowledges the inspiration and continuous support by P. Dimitriou and S. Goriely. This work was performed within an IAEA Nuclear Data Section Special Service Agreement.

References:

[1] G.A. Bartholomew *et al.*, Adv. Nucl. Phys. **7** (1973) 229.`

[2] C.M. McCullagh, PhD thesis, Stony Brook, (1979) and C.M. McCullagh, M. Stelts and R.E. Chrien, Phys. Rev. C**23**, 1394 (1981).

[3] J. Kopecky and M. Uhl, "Present status of experimental gamma-ray strength functions", ECN Report ECN-RX—94-103 (1994).

[4] IAEA-TECDOC-1034 "Handbook for Calculations of Nuclear Reaction Data, Reference Input Parameter Library (1998)

[5] IAEA-TECDOC-1506 "Handbook for calculations of nuclear reaction data, RIPL-2" (2006) p. 117

[6] A.V.Ignatyuk, *et al,* in RIPL-3 documentation, R. Capote, *et al.*, Nucl. Data Sheets **110 (**2009) 3107.

[7] S.F. Mughabghab, "Atlas of Neutron Resonances" (Elsevier 2006).

[8] J. Kopecky, "Present status of experimental gamma-ray strength functions derived from neutron capture", IAEA Report INDC(NED)-013 (2016).
[9] S.F. Mughabghab, "Atlas of Neutron Resonances" (Elsevier 2018).
[10] Evaluated Nuclear Data Structure File, https://www.nndc.bnl.gov/ensdf/
[11] J. Kopecky, "Atlas of average resonance capture data (Starter file)", IAEA report INDC(NDS)-0738 (2017).
[12] R.E. Chrien, "Neutron resonance averaging with filtered beams", Report BNL-36646 (1985)
[13] F. Becvar et al., J. of Nucl. Phys. **46** (1987) 3, in Russian
[14] F. Becvar et al., *Proc. Of the Int. Conference on Neutron Physics,* Kiev (1988) p.8
[15] F. Becvar et al., Yad.Fiz. **46** (1987) 392
[16] R.E. Chrien and J. Kopecky, Phys. Rev. Lett. **39** (1977) 911
[17] J. Kopecky et al., Nucl. Phys. A**334** (1980) 35
[18] R .E. Chrien and J. Kopecky, Phys. Rev. C**1** (1970) 973
[19] J. Kopecky, M. Uhl and R.E. Chrien, Phys. Rev. C**47** (1993) 312
[20] S. Goriely *et al.* , Phys.Rev. C**94** (2016) 044306

Appendix:

DRC Data Sources:

[1] M.J. Kenny et al., Austr.J.Phys. 27 (1974) 759 *F-20, Al-28, S-33*

[2] I. Bergqist et al., Phys.Rev. 158 (1967) 1049 *Mg-25, Al-28*

[3] C.M. McCullagh, PhD thesis, Stony Brook, (1979) and C.M. McCullagh, M. Stelts and R.E. Chrien, Phys. Rev. C23, 1394 (1981) *Al-28, Cl-36, Pd-106, Te-126, I-128, Ba-136, Nd-144, Lu-176, Ta-182, W-184, Pt-196, U-237*

[4] M.J. Kenny et al., Nucl.Phys. A170 (1976) 164 *Si-28,30*

[5] R.E. Chrien and J. Kopecky, Phys.Rev.Lett. 39 (1977) 911 *Cl-36*

[6] H.I. Liou and R.E. Chrien, *Proceedings of the 3rd International Symposium on Neutron Capture γ-ray Spectroscopy and Related Topics,* (Plenum, New York, 1979) p.67 *Sc-46*

[7] J. Kopecky et al., Nucl.Phys. A334 (1980) 35 *Cr-52*

[8] C. Coveva, Il Nuovo Cimento A 101 (1994) 85 *Cr-54*

[9] R.E. Chrien et al., Phys.Rev. C1 (1970) 973 *Fe-57*

[10] J.C. Wells Jr. Et al., Phys.Rev. C18 (1978) 707 *Fe-59*

[11] O. Wasson et al., Phys.Rev. 176 (1968) 1314 *Co-60*

[12] W. Stein et al., Phys.Rev. C1 (1969) 1468 *Cu-64*

[13] R.E. Chrien et al., Phys.Rev. C9 (1974) 1839 *Ge-74*

[14] R.E. Chrien et al., Phys.Rev. C3 (1971) 2054 *Nb-94*

[15] O.A. Wasson and G.C. Slaughter, Phys.Rev. C8 (1973) 297 *Mo-93*

[16] R.E. Chrien et al., Phys.Rev. C13 (1976) 578 *Mo-99*

[17] K. Rimavi et al., Phys.Rev. C9 (1974) 1978 *Ru-100, 102*

[18] C. Coceva et al., Nucl.Phys. A385 (1982) 301 *Ru-100,102*

[19] K. Rimavi et al., Phys.Rev. C2 (1970) 1793 *Rh-104*

[20] C. Coceva et al., Nucl. Phys. A170 (1971) 153 *Pd-106*

[21] F. Corvi and M. Stefanon, Nucl.Phys. A233 (1974) 185 *In-116*

[22] A. Lottin and D. Paya, J.Phys. (Paris) 32 (1971) 849 *Sb-122, Sb-124*

[23] S. Raman, private communication *Nd-146*

[24] F. Becvar et al., J. of Nucl.Phys. (Russian) 46 (1987) 3 *Sm-148*

[25] F. Becvar et al., Nucl.Phys. A236 (1974) 198 *Sm-150*

[26] F. Becvar et al., *Capture Gamma-Ray Spectroscopy,* (Inst. Of Physics Conference Series 88, Bristol 1988) p. 649 and private communication *Sm-150, Gd-153, Gd-157,159, Lu-177*

[27] F. Becvar et al., *Proc. Of the Int. Conference on Neutron Physics,* Kiev (1988) p.8 *Gd-155*

[28] C. Granja et al., Nucl.Phys. A729 (2003) 679 *Gd-159*

[30] S. Kahane et al., Phys.Rev. C30 (1984) 807 *Er-168*

[31] J.B. Garg et al., Phys.Rev. 174 (1968) 1139 *Er-169*

[32] M.A. Lone et al., Phys.Rev. 174 (1968) 1512 *Tm-170*

[33] O. Wasson and R.E. Chrien, Phys.Rev. C2 (1970) 675 *Lu-176*

[34] F. Becvar et al., Yad.Fiz. 46 (1987) 392 *Lu-176,177, Yb-174*

[35] M. Stefanon and F. Corvi, Nucl.Phys. A281 (1977) 240 *Hf-178*

[36] M.L. Stelts et al., Phys. Rev C16 (1977) 574 *Ta-182*
[37] S. Samour et al., Nucl.Phys. A121 (1968) 65 *Pt-196*
[38] O.A. Wasson et al., Phys.Rev. 173 (1968) 1170 *Au-198*
[39] M.A. Lone et al., Nucl.Phys. A243 (1975) 413 *Hg-198,199,202*
[40] B.K.S. Koene and R.E Chrien, Phys.Rev C16 (1977) 588 *Th-233, U-235*
[41] R.G. Graves et al., Phys.Rev. C8 (1973) 781 *U-236*
[42] T. von Egidy et al., Phys.Rev. C6 (1972) 266 *U-237*
[43] O.A. Wasson et al., Phys.Rev. C4 (1971) 900 *U-239*
[44] R.E. Chrien et al., Nucl.Phys. A436 (1985) 205 *Pu-240*
[45] L. Zanini et al., Phys.Rev. C68 (2003) 014320 *Ag-108*

Nuclear Data Section
International Atomic Energy Agency
Vienna International Centre, P.O. Box 100
A-1400 Vienna, Austria

E-mail: nds.contact-point@iaea.org
Fax: (43-1) 26007
Telephone: (43-1) 2600 21725
Web: http://nds.iaea.org